CXCL12 chemokine dimer signaling modulates acute myelogenous leukemia cell migration through altered receptor internalization

Donovan Drouillard[1,2,#], Michael Halyko[2,3,#], Elizabeth Cinquegrani[2,#], Maria Poimenidou[1,2], Miracle Emosivbe[4], Donna McAllister[1,2], Francis C. Peterson[4], Adriano Marchese[4], and Michael B. Dwinell[1,2,5,*]

[1]Department of Microbiology & Immunology, [2]Center for Immunology, [3]Department of Pediatrics, [4]Department of Biochemistry, [5]Department of Surgery, Medical College of Wisconsin, Milwaukee WI, USA

*, corresponding author

#: these authors contributed equally

Correspondence:
Michael B. Dwinell, PhD
Professor of Microbiology & Immunology and Surgery
Director of the Center for Immunology
Medical College of Wisconsin
8701 Watertown Plank Road
Milwaukee, WI 53122
Phone: 414-955-7427
Email: mdwinell@mcw.edu

ABSTRACT

Acute myeloid leukemia (AML) is a malignancy of immature myeloid blast cells with stem-like and chemoresistant cells being retained in the bone marrow through CXCL12-CXCR4 signaling. Current CXCR4 inhibitors that mobilize AML cells into the bloodstream have failed to improve patient survival, likely reflecting persistent chemokine receptor localization on target cells. Here we characterize the signaling properties of CXCL12-locked dimer (CXCL12-LD), a bioengineered variant of the naturally occurring oligomer of CXCL12. CXCL12-LD, in contrast to wild-type or locked monomer variants, was unable to induce chemotaxis in AML cells. CXCL12-LD binding to CXCR4 decreased G protein, β-arrestin, and intracellular calcium mobilization signaling pathways, and indicated the locked dimer is a partial agonist of CXCR4. Despite these partial agonist properties, CXCL12-LD increased CXCR4 internalization compared to wildtype and monomeric CXCL12. Analysis of a previously published AML transcriptomic data showed CXCR4 positive AML cells co-express genes involved in survival, proliferation, and maintenance of a blast-like state. The CXCL12-LD partial agonist effectively mobilized stem cells into the bloodstream in mice suggesting a potential role for their use in targeting CXCR4. Together, our results suggest that enhanced internalization by CXCL12-LD partial agonist can avoid pharmacodynamic tolerance and may identify new avenues to better target G protein coupled receptors.

Keywords:

Chemokines, CXCR4, Acute Myeloid Leukemia, GPCR, receptor internalization, cell signaling

INTRODUCTION

The chemokine CXCL12 can self-associate into dimers at high concentrations or following interactions with its cognate receptors or glycosaminoglycan binding partners [1]. To determine the impact of ligand oligomerization on chemokine function the Volkman group has engineered CXCL12 into variants locked into either a dimeric structure, CXCL12-locked dimer (CXCL12-LD) or a monomer form, CXCL12-locked monomer (CXCL12-LM) [2]. These forms are structurally identical to native CXCL12 conformations attained by oligomerization of the wild-type protein and retain the ability to bind to and activate the cognate receptor CXCR4 or the atypical chemokine receptor 3 (ACKR3) [3]. Recognizing that chemotaxis typically follows a biphasic response CXCL12-LD and CXCL12-LM were used to uncover discrete functional roles for the monomer in stimulating cell migration, compared to the dimer, which induced a stationary phenotype we termed “ataxis” [4, 5]. Thus, our data from cell culture models suggest that CXCL12 induced chemotaxis, with maximal migration observed in a narrow concentration range of ligand, reflects formation of dimers at high concentrations. *In vivo*, CXCL12-mediated chemotaxis regulates the trafficking of CXCR4-expressing hematologic cells into primary and secondary lymphoid tissues, angiogenesis, and is a key component in solid cancers for promoting metastasis [6, 7]. In hematological malignancies, CXCR4 is thought to function less in chemotactic migration and more as a retention signal that keeps malignant cells within the bone marrow where they are protected from chemotherapy [8]. While we have previously dissected CXCL12 signaling in colon, breast, and pancreas solid tumors [9-11], the pharmacologic properties of monomeric and dimeric ligands in hematological malignancies, such as acute myeloid leukemia (AML), remains unknown.

AML is a heterogenous malignancy of adults and children characterized by clonal expansion of immature myeloid blast cells with resulting bone marrow failure and ineffective erythropoiesis [12]. The standard of care chemotherapy regimen during induction therapy consists of daunorubicin and cytarabine. This regimen is relatively effective in younger patients

with a 5-year survival rate of 55% [13], but ineffective in older patients with a 5-year survival rate of only 17% in patients greater than 60-years-old due to a lower tolerance for high-dose chemotherapies [14]. With a median diagnosis age of 68 years [15], there is a pressing need to develop new, non-cytotoxic therapies to treat AML in the elderly. An attractive therapeutic target in the leukemia microenvironment is the CXCL12-CXCR4 chemokine axis, which helps maintain AML cells in their protective bone marrow niche [16]. AML cell lines variably increase CXCR4 expression upon chemotherapy treatment, resulting in increased CXCL12-mediated chemotaxis and conferring a bone marrow stroma-mediated survival advantage [17]. In preclinical models with human AML xenografts, AMD3100, a clinically available inhibitor of CXCR4 known by the trade name Plerixafor, combined with chemotherapy demonstrated chemosensitizing effects supporting a role for the CXCL12-CXCR4 axis as a mediator of stromal-dependent chemo-resistance [18, 19]. In addition, a number of small peptide CXCR4 antagonists have been studied in preclinical mouse models and have shown similar chemosensitizing effects through a variety of pathways including mobilization of AML cells into the peripheral blood [20], activation of pro-apoptotic pathways [21, 22], or inhibition of proliferation [20]. Despite this preclinical success, phase I/II clinical trials combining AMD3100 with a variety of chemotherapy regimens in adults with AML have found little to no clinical benefit [22-25].

Clinical trials with the newer generation of CXCR4 inhibitors were, as with AMD3100, terminated due to their lack of efficacy [26, 27]. The failure of current CXCR4 inhibitors highlights the need to better understand the signaling mechanisms whereby CXCL12 and CXCR4 regulate AML functions. Using rationally designed and engineered CXCL12 variants locked into their dimeric structure we have uncovered that the dimer is a partial agonist of CXCR4 that stimulates ligand-induced receptor internalization that is stronger and more sustained compared to monomer or wild-type ligand. This internalization occurs independent of chemotaxis as the dimer was unable to stimulate cell migration, despite retention of G protein signaling and β-arrestin recruitment. The sustained internalization of CXCR4 by dimeric ligand

suggests a new pathway to disrupt CXCL12-mediated retention of AML within the protective bone marrow niche.

RESULTS

Human AML cell lines are CXCR4+ and migrate to CXCL12-WT but not CXCL12-LD

As a first step to investigate mechanisms of chemokine signaling in AML cells, we used RT-PCR and flow cytometry to assess the expression of CXCR4, the cognate receptor for CXCL12 in three human AML cell lines. Consistent with a prior report, CXCR4 mRNA (**Fig. 1A**) and protein (**Fig. 1B**) was highly expressed in three different AML cells [28]. Transcript for ACKR3, an atypical chemokine receptor CXCL12 may also bind, was also detected on each of the AML cell lines (**Supplemental Fig. 1A**).

Accumulating evidence from our lab and others support a model wherein the biphasic chemotactic migration induced by chemokines may reflect distinct binding modes of monomeric and dimeric forms of the chemokine. In the CXCL12 model, chemotaxis reflects receptor activation by ligand monomers, with dimer formation becoming predominant as the concentration of the ligand increases, shifting the cells to ataxis. Consistent with that model, AML cells undergo dose dependent migration in response to CXCL12-WT protein with an optimal concentration of approximately 30 nM (**Fig. 1C, 1D**). Concentrations above 80 nM resulted in a less robust chemotactic response, consistent with the expected bell-shaped chemotactic curve due to possible CXCL12-WT dimerization at higher concentrations. In contrast to wild-type or monomeric variants, data from transwell migration assays in two separate AML cell lines indicate that CXCL12-LD was unable to stimulate migration at 3, 30, or 300 nM concentrations (**Fig. 1E, 1F**). However, we did not observe a difference between CXCL12-WT and a variant locked into a monomer and unable to form dimers, CXCL12-LM [10].

Prior CXCL12 structure-function analysis established a substantial role for the first two amino acids in the ligand amino terminus, Lys1 and Pro2, in receptor activation, with a complete loss of Ca^{2+} flux agonist activity upon deletion or substitution of either residue [29]. Previous work with a CXCL12 variant lacking these first two residues ($CXCL12_{3–68}$) suggest that this

molecule binds to CXCR4, albeit with reduced affinity [11, 29]. Consistent with those data, $CXCL12_{3-68}$ failed to induce chemotaxis at any concentration (**Supplemental Fig. 1B, 1C**).

CXCL12 G protein signaling and arrestin recruitment

CXCR4 activates heterotrimeric G proteins, leading to inhibition of adenylyl cyclase and mobilization of intracellular calcium. As shown in **Figure 2**, we first assessed $G_{\alpha i}$ signaling in THP-1 cells treated with CXCL12-WT, CXCL12-LD, or $CXCL12_{3-68}$. Consistent with its binding to $G_{\alpha i}$-coupled CXCR4, CXCL12-WT inhibited cAMP production in a dose-dependent manner with significant inhibition occurring at a concentration of 1000 nM (**Fig. 2A**). While the dimer was unable to promote chemotaxis, CXCL12-LD inhibited cAMP production at 1000 nM **(Fig. 2A**, dark grey bar) while $CXCL12_{3-68}$ failed to activate the receptor (**Fig. 2A, light grey bar**).

To analyze another output of GPCR activation we measured intracellular calcium mobilization. We found that both CXCL12-LD and CXCL12-WT induced intracellular calcium flux in THP-1 and U937 AML cell lines (**Fig. 2B, 2C**). CXCL12-LD induced calcium flux but with less potency and efficacy than CXCL12-WT. To confirm if calcium flux was mediated by activation of the $G_{\alpha i}$ subunit of the GPCR, we performed the same experiment on cells treated in the presence or absence of pertussis toxin, which ADP-ribosylates $G_{\alpha i}$ to prevent the activation of the G protein. CXCL12-induced calcium flux was extinguished by the addition of pertussis toxin (**Fig. 2D**), demonstrating ligand activation of CXCR4 mediates calcium flux through activation of the $G_{i/o}$ family of proteins.

In addition to G protein signaling, CXCL12 binding to CXCR4 induces β-arrestin recruitment. Using bioluminescence assays, we measured the recruitment of β-arrestin to CXCR4 following treatment with either CXCL12-WT, CXCL12-LM, or CXCL12-LD. Compared with wild-type or monomer ligand, CXCL12-LD recruited β-arrestin with less potency over a 20 minute time course (**Supplemental Fig. 2, left panels**). Similarly, using a mini-$G_{\alpha i}$ BRET we

confirmed the lower calcium mobilization evoked by CXCL12-LD and found that the dimer less potently activated the CXCR4 G protein complex (**Supplemental Fig. 2, right panels**). Data from each of the individual G-protein and arrestin BRET experiments were then used to calculate the transduction efficiencies for each (**Fig. 2E**). Lastly, the bias factors were calculated for each ligand, with a bias factor of ≥5 indicative of a biased agonist [30]. The calculated bias factors demonstrated that CXCL12-LD signals as a balanced partial agonist while CXCL12-LM is a balanced full agonist in relation to CXCL12-WT (**Fig. 2F**) in AML cells.

β-arrestin recruitment requires phosphorylation of Ser/Thr residues in the CXCR4 C-terminus. The intracellular CXCR4 C-terminus has 18 Ser/Thr residues whose site-specific phosphorylation is dynamically regulated by G protein regulatory kinases (GRKs) [31]. As a first step, we used a phospho-specific antibody against dually phosphorylated Ser324 and Ser325 (Ser324/325) of the CXCR4 C-terminal tail. Compared to vehicle treated CXCR4 transfectants (**Fig. 3A**), cells treated with 10 nM CXCL12-WT (**Fig. 3B**) or CXCL12-LM (**Fig. 3C)** had increased CXCR4 phosphorylation at Ser324/325. In contrast, CXCL12-LD resulted in weak CXCR4 C-terminal serine phosphorylation (**Fig. 3D**). Altogether, these data support the notion that CXCL12-LD is a partial agonist that has lower potency and efficacy at signaling through either $G_{\alpha i}$ and β-arrestin.

CXCL12-LD internalizes CXCR4 more effectively than CXCL12-WT

Canonical GPCR internalization occurs largely through β-arrestin dependent signaling mechanisms and has been measured for CXCL12-WT in a variety of cells including human T cells and the rat basophilic leukemic cell line RBL-2H3 [32, 33]. Current antagonists of CXCR4 signaling do not internalize the receptor, likely reflecting their functioning as competitive inhibitors occupying a key ligand binding site [33-35]. Despite the dimer's limited recruitment of β-arrestin, we measured a significant dose-dependent decrease in CXCR4 surface localization

in cells treated with CXCL12-LD at both 30 minutes and 24 hours (**Fig. 4A, 4B**). The 12G5 monoclonal antibody binds CXCR4 at the 2nd extracellular loop, a process that may be blocked when different agonists are bound to the receptor [36]. To more stringently evaluate if the receptor was being internalized, we repeated the experiment using monoclonal antibody clone 1D9, an antibody that binds the N-terminus of the receptor and can therefore detect both ligand-bound and un-bound CXCR4 [37]. Just as with 12G5, we measured decreased surface levels of CXCR4 after 30 minutes (**Fig. 4C**) and 24 hours (**Fig. 4D**) of CXCL12-WT, CXCL12-LM, or CXCL12-LD treatment. Both 12G5 and 1D9 antibodies detected a statistically significant decrease in CXCR4 on the surface of cells treated for 24 hours with CXCL12-LD, but not CXCL12-LM, compared to CXCL12-WT treated cells. Moreover,1D9 measured a significant internalization of CXCR4 at 30 minutes that was sustained through 24 hours. CXCR4 internalization was next measured in THP-1 and AML193 cell lines treated with 100 nM CXCL12-WT, CXCL12-LM, or CXCL12-LD and confirmed the larger and more sustained internalization induced by the dimer variant (**Fig. 4E, 4F**). Lastly, as we had shown decreased CXCR4 C-terminal phosphorylation of S324/325 needed for arrestin-receptor interactions, we measured CXCR4 internalization in CXCR4-FLAG transfected HeLa cells. Consistent with our data in AML cells, antibody against the N-terminal FLAG tag confirmed increased internalization with CXCL12-LD relative to wild-type protein or CXCL12-LM (**Supplemental Fig. 3**).

As the three AML cell lines express both CXCR4 and ACKR3, we next asked if the ligand variants modified internalization of the atypical chemokine receptor. ACKR3 functions as a scavenger receptor that helps sculpt the chemokine gradient without directly invoking cellular migration [38] and is an arrestin-biased receptor in response to CXCL12 [39]. Unlike the internalization measured for CXCR4, none of the CXCL12 oligomers induced internalization of ACKR3 in U937, THP-1, or AML-193 cells (**Supplemental Fig. 4**).

As an additional measure to verify that the decreased surface CXCR4 staining measured by flow cytometry was not due to steric hindrance of the binding site by CXCL12-LD,

we generated CXCL12 variants with AzDye647 conjugated to the ligands C-terminal tail. U937 cells treated with fluorescent dye tagged CXCL12-WT, CXCL12-LM, or CXCL12-LD for 30 minutes demonstrated robust internalization of the ligand (**Fig. 5A-C**). Significantly more CXCL12-LD-AzDye647 was detected within U937 cells compared to wild-type or monomeric chemokine (**Fig. 5D**). These fluorescence microscopy data support the notion that CXCL12-LD promotes receptor internalization rather than sterically hindering CXCR4 antibodies from binding.

Partial agonist CXCL12-LD but not CXCR4 antagonists stimulate receptor internalization

Previous reports suggest CXCR4 small molecule antagonists induce therapeutic resistance when used to treat patients [23-27]. Conventional wisdom is that therapeutic resistance reflects an upregulation of the receptor by the antagonist [40-44]. To test that notion, CXCR4 surface levels were measured in U937 (**Fig 6A, 6B**) or AML-193 (**Fig 6C, 6D**) cells treated with the receptor antagonists AMD3100 or BL-8040 and compared against cells incubated with CXCL12-LD. CXCR4 levels were increased in cells treated with AMD3100 or BL-8040 at both the 30 minute and 24 hour treatment (**Fig. 6A, 6B**). AML-193 cell showed a more modest increases in surface CXCR4 after 24 hours of treatment with AMD3100 or BL-8040 (**Fig. 6C, 6D**). These data are in stark contrast to CXCL12-LD treated cells, in which CXCR4 surface levels were significantly reduced in both U937 and AML-193 cells at both time points.

CXCR4 is upregulated in chemoresistant AML blasts

The unique ataxic and internalizing properties of CXCL12-LD prompted further investigation into the potential for the dimer to influence AML *in vivo*. CXCR4 is important for trafficking and retention of hematopoietic cells in the bone marrow [45]. To analyze the CXCR4 expressing cells in AML patients, we turned to publicly available large single-cell RNA datasets. Using a dataset that contains bone marrow aspirates of 16 AML patients [46], we found CXCR4

expression was enriched myeloid lineage cells (**Fig. 7A**). To examine if CXCR4 was upregulated in malignant monocytes compared to healthy monocytes, we compared the monocyte-like cells, which have a confirmed mutation in targeted sequences known to be mutated in AML, to healthy, non-mutated monocytes from the same donors. CXCR4 expression was found to be upregulated in the malignant monocytes compared to the healthy monocytes (**Fig. 7B**). Next, we investigated transcriptional differences between CXCR4 positive and negative malignant monocytes in AML patients. CXCR4+ cells had upregulated expression of the transcription factor JUN and transcriptional coactivator CITED2, each of which are necessary for AML blast survival [47-49] (**Fig. 7C**). Further, HLX and SAP30, two proteins important for blocking differentiation and enhancing proliferation, respectively, were similarly elevated in malignant CXCR4+ AML [50-52]. These gene correlations were confirmed with the AML PanCancer Atlas dataset on cBioPortal (**Supplemental Fig. 5**). Lastly, as some transcription factors are lowly expressed and thus difficult to detect by single cell RNA analysis [53], we completed analyses using the CollecTRI R package [54]. ETV5 and FOXH1 were within the top results in the CXCR4+ group, both of which are important for preventing differentiation and maintaining a blast-like state in AML [55, 56] (**Fig. 7D**). Together these data suggest that CXCR4 is upregulated in AML and that CXCR4+ AML blasts similarly upregulated genes associated with resisting apoptosis, proliferation, and maintaining and a stem-like state.

CXCL12-LD mobilizes monocytes and CXCR4+ hematopoietic stem cells in mice

Small molecular receptor antagonists of CXCR4 are hypothesized to chemosensitize AML cells through mobilization of AML blasts into the peripheral blood [18, 26, 49]. AMD3100 was the first bicyclam CXCR4 antagonist shown to increase the concentration of circulating hematopoietic stem cells in mouse models [19]. To date, however, AMD3100 has had limited success in clinical trials of AML, resulting in no improvement in remission rates compared to historical controls and indicating a need for further exploration of CXCR4 therapeutic targeting

[26]. To determine if chemokine oligomers can mobilize CXCR4-expressing cells *in vivo*, wild-type C57BL/6 mice were injected subcutaneously with CXCL12-LD and blood was collected after two hours to assess monocyte mobilization and after four hours to assess CXCR4+ hematopoietic stem cell mobilization. We observed an increase in circulating monocytes in CXCL12-LD treated mice compared to vehicle treated mice (**Fig. 7E**). Further, there was an increase in the percentage of CXCR4+ circulating hematopoietic stem cells (**Fig. 7F**). These data support the hypothesis that CXCL12-LD promotes long-term mobilization of CXCR4-expressing cells into the peripheral blood and could be used to remove AML blasts out of the chemoprotective bone marrow niche.

DISCUSSION

Cumulatively, our data support the summary model in **Figure 8** suggesting that retention of hematopoietic or transformed cancer cells in the bone marrow may be disrupted by the unique signaling properties of the partial agonist CXCL12-LD. Using reductionist AML cell culture models, we determined that CXCL12-LD, compared to wild-type or monomeric ligand, is a partial agonist of CXCR4. We observed increased internalization of CXCR4 and not ACKR3 with CXCL12-LD and a complete inability to evoke chemotaxis. In comparison to other inhibitors of CXCR4 chemotaxis, AMD3100 is a 1st generation CXCR4 inhibitor that likely functions as a competitive antagonist and both LY2510924 and BL-8040 (Motixafortide, T140, BKT140) are 2nd generation CXCR4 inhibitors that function as inverse agonists with higher potency compared to AMD3100 [57, 58]. While AMD3100, BL-8040, and CXCL12-LD all block chemotaxis, only CXCL12-LD reduced surface CXCR4 expression while both AMD3100 and BL-8040 increase it. As both chemotaxis and receptor internalization have been canonically linked with β-arrestin signaling [32] our data suggest a new mechanism for homologous CXCR4 desensitization and a potential avenue for avoiding resistance to CXCR4 inhibitors.

Prior studies of CXCL12-WT show it engages with CXCR4 at four different sites on the receptor, or chemokine recognition sites (CRS) [59]. CXCL12-WT binds CRS0.5, 1.0, 1.5, and 2.0 while CXCL12-LD can bind all but CRS0.5 [60, 61]. However, the inability to bind CRS0.5 is thought to only affect signaling efficacy, suggesting that CRS0.5 is required for full ligand agonism [60]. The lack of CXCL12-LD binding to CRS0.5 supports the idea that the decreased CXCR4 1D9 antibody binding measured is not due to steric hindrance by the CXCL12-LD agonist, as the 1D9 antibody clone binds the flexible N-terminus and CRS0.5 is within the distal N-terminus of the receptor [62]. Another distinction between CXCL12-LD and CXCL12-WT binding occurs when examining post-translational CXCR4 tyrosine sulfation. Both CXCL12-LD and CXCL12-WT can bind sulfated residues Tyr-21 and Tyr-12 on the CXCR4 amino terminus, while CXCL12-LD differs from wild-type ligand by binding to sulfated Tyr-7 [3, 63]. Additionally, sulfated Tyr-21 binds CXCL12-LD with 20-fold stronger affinity than CXCL12-WT or CXCL12-LM and sulfated Tyr-21 promotes ligand dimerization [3]. These discrete differences in ligand oligomer interactions with CXCR4 may help explain the discrepancy between cellular migration and receptor internalization. CXCL12-LD binds the receptor in a dimerized state, while CXCL12-WT likely binds as a monomer and then dimerizes [3]. This difference in sequential binding and dimerization may explain why dimer binding to CXCR4 stimulates pronounced and durable internalization in the absence of chemotactic migration.

Another quandary posed by our data is the increased internalization with CXCL12-LD despite decreased β-arrestin recruitment. β-arrestin independent internalization of GPCRs has been observed previously and can occur through multiple mechanisms *via* clathrin coated pits [64]. New studies suggest that CXCR4, but not all GPCRs, are internalized through sorting nexins (SNX) and particularly SNX9 and SNX18 [65]. This process was shown to be partially driven by the phosphorylation of residues on the proximal CXCR4 C-terminus. The phosphorylation sites required to recruit SNX9 are different from those required for β-arrestin, in

line with our data suggesting reduced β-arrestin recruitment but increased internalization by CXCL12-LD. While we show decreased phosphorylation of residues Ser324/325, we did not examine Ser338/339 in the proximal cluster which could be driving SNX9 recruitment and CXCR4 internalization. Further, β-arrestin binding and SNX9 binding to CXCR4 are thought to be mutually exclusive [65]. A decrease in β-arrestin binding, as seen with CXCL12-LD, could allow for increased SNX9 binding and internalization.

Overexpression of CXCR4 has been demonstrated in a variety of hematologic and solid cancers including AML [17, 66, 67]. While preclinical experiments implicate CXCR4 antagonism as a promising means of chemosensitizing AML and other hematologic malignancies, clinical results have shown limited efficacy [27, 67, 68]. A shared feature of these CXCR4 antagonists is blockade of ligand binding and downstream functional activity. As shown here, AMD3100 and other small molecule antagonists known to inhibit receptor signaling may paradoxically increase receptor surface levels, which in turn negates the benefit sought in blocking receptor signaling, a process known as “antagonist tolerance”. Antagonist tolerance can also be seen in other GPCRs and may be a key contributor to treatment resistance and the lack of clinical benefit seen with AMD3100 [40-44, 69-71]. Extrapolating from those *in vitro* data would suggest that AML tolerance to CXCR4 inhibition through persistent surface localization of receptor occurs within a crucial time-window preceding the completion of the initial week-long induction chemotherapy. Using an engineered protein to dissect pharmacological signaling of CXCR4 we have extended our initial discovery of partial agonism in pancreas cancer cells to a high-risk hematologic malignancy to examine how agonists of the same receptor function. The differential ability of CXCL12-LD to promote receptor internalization provides a potential avenue to address roles in pharmacotherapy that traditional antagonists have been unable to address.

MATERIALS and METHODS

Cell Lines

Human U937 (CRL-1593.2) and THP-1 (TIB-202) cells were obtained from the ATCC (Manassas, VA) and maintained in RPMI with L-glutamine and 25 mM HEPES (Life Technologies Inc, Carlsbad, CA) supplemented with 10% (v/v) fetal bovine serum (Omega Scientific, Tarzana, CA). HEK-293 epithelial cells (CRL-1573) and HeLa cells (CCL-2) purchased from the ATCC were maintained in DMEM (Life Technologies Inc) supplemented with 10% (v/v) fetal bovine serum (Omega Scientific). Human AML-193 (CRL-9589) cells were obtained from the ATCC and maintained in IMDM supplemented with 5% (v/v) fetal bovine serum, 1X Insulin-Transferrin-Selenium (Gibco), and 5 ng/mL GM-CSF (R&D Systems). Cell lines were authenticated annually using short tandem repeat profiling and mycoplasma-tested semi-annually. HEK293 cells were transfected with HA-CXCR4 using TransIT-LT1 transfection reagents (Mirus Bio, Madison, WI) as previously described [72]. HeLa cells were transiently transfected using polyethylenimine as previously defined [73].

Recombinant Chemokines

CXCL12 wild-type (CXCL12-WT), locked monomer (CXCL12-LM), locked dimer (CXCL12-LD) and NH_2-terminal truncation ($CXCL12_{3-68}$) variants were expressed and purified as previously described [10, 74]. The CXCL12-LD mutations are L36C and A65C and create a dimeric protein [2, 11]. The CXCL12-LM mutations are L55C and I58C [10, 69]. The engineered locked dimer or locked monomer proteins are structurally indistinguishable from native dimeric and monomeric protein, respectively, and retain full CXCR4 receptor binding capability [4, 10]. Proteins were expressed in *E. coli* and bacterial cells lysed by French press. Fusion protein was purified through nickel chromatography, refolded by infinite dilution, and ULP1 protease was used to cleave the 6XHIS-Sumo tag. CXCL12-WT and CXCL12-LD were fluorescently labeled with AzDye647 using a two-step process employing sortagging [75] and copper-catalyzed azide-alkyne click chemistry as defined previously [76]. The identity of native or fluorescently

labeled CXCL12 was confirmed by linear ion trap quadrupole mass spectrometry. Lyophilized proteins were stored at −20°C.

Flow Cytometry

THP-1, U937, and AML-193 cells were passaged to 5 x 10^5 cells/mL the day prior to experiment. Cells were washed twice using cold PBS, incubated in Fc blocking solution (Miltenyi Biotec, Bergisch Gladbach, Germany), and washed twice. Cells were then incubated for 30 minutes in fluorophore conjugated primary CXCR4 antibody (Invitrogen, Waltham, MA) on ice and washed twice. Fluorescence intensity was measured on a BD-LSR II flow cytometer and analyzed by FlowJo software (BD Biosciences, San Jose, CA).

RT-PCR

RNA was isolated using the RNA Easy kit from Qiagen and treated with DNAse I to remove genomic DNA contaminants. Conversion to cDNA was performed by priming with random hexamers and the SuperScript II cDNA synthesis kit (Life Technologies). PCR products were separated by agarose gel electrophoresis and visualized by ethidium bromide staining and ultraviolet imaging. Primers for actin were used as a loading control. Amplification of chemokine receptors was done using the following primers (5′-3′):

Human CXCR4 Forward 5'-GACTCCATGAAGGAACCCTGTTTCCG-3'

Human CXCR4 Reverse 5'-CTCACTGACGTTGGCAAAGATGAAGTCG-3'

Human β-actin Forward 5’-ACCCACACTGTGCCCATCTACG-3’

Human β-actin Reverse 5’-AGTACTTGCGCTCAGGAGGAGC-3’.

Human ACKR3 Forward 5’-GTGGTGGTCTGGGTGAATATC-3’

Human ACKR3 Reverse 5’-GATGTAGTGCAGGATGGAGAAG-3’

cAMP Quantification

THP-1 cells were grown in a T-75 flask, then counted immediately prior to the measurement of cAMP using a competitive enzyme immunoassay as we have shown before [77]. THP-1 (5×10^5) cells were aliquoted into 1.5 mL tubes and stimulated with 10 mM 3-isobutyl-1-methylxanthine (IBMX) for 30 minutes at room temperature, after which they were incubated with either CXCL12-WT, CXCL12-LD, or CXCL12-3-68 for an additional 10 minutes. Cells were then stimulated for 10 minutes with 10 μM forskolin (FSK) to stimulate cAMP production. Controls included unstimulated cells and cells treated with IBMX and FSK alone. Cells were then centrifuged and incubated with 0.1 M HCl for 20 minutes before being centrifuged (300 x g on microcentrifuge) for 10 minutes. Supernatant was isolated, and cAMP was assayed using a competitive enzyme immunoassay kit (Cayman Chemical Co., Ann Arbor, MI) according to the manufacturer's instruction manual. Fluorescence was measured at room temperature with a SpectraMax Multimode Microplate reader (Molecular Devices, San Jose, CA) at a wavelength of 450 nm. Readings were graphed and analyzed according to the immunoassay instruction manual.

Calcium Mobilization

Calcium mobilization was measured using the FLIPR Calcium 6 assay kit (Molecular Devices) according to manufacturer's directions. Cells were plated to 50,000 cells/well in 96-well plates. Cells were washed with Calcium/Magnesium-free HBSS supplemented with 20 mM HEPES (Thermo Fisher Scientific, Waltham, MA) and 0.1% (v/v) BSA Fraction V (Thermo Fisher Scientific) and loaded with Calcium-6 dye for 1 hour at 37°C and 5% CO_2. Chemokines were diluted in calcium/magnesium-free HBSS buffered with 20 mM HEPES and were then loaded onto a separate compound plate. Fluorescence was measured at 37°C with a FlexStation3 Multimode Microplate Reader (Molecular Devices) with excitation and emission wavelengths of 485 and 515 nm, respectively. Chemokines were resuspended at the

concentrations indicated in the figure legends and added to the cells after baseline fluorescence was measured for 20 seconds. The percentage Ca^{2+} flux was calculated from the maximum fluorescence minus the minimum fluorescence as a percent of baseline fluorescence. EC_{50} values were determined by nonlinear fitting to a four-parameter logistic function. For experiments with addition of the Gα subunit inhibitor, cells were treated with 100 ng/mL pertussis toxin for 4 hours prior to assessing calcium flux in response to 500 nM CXCL12-WT or CXCL12-LD.

Confocal Immunofluorescence Microscopy

Phosphorylated CXCR4 serine residues 324 and 325 were detected in HeLa cells as described previously [78], grown on 10 cm dishes were transfected with 5 μg of HA-CXCR4-YFP and passed 24 hours later onto coverslips pretreated with poly-l-lysine, as described previously [79]. Cells were washed once with DMEM plus 20 mm HEPES and serum-starved for 3-4 hours in the same medium, followed by 30-minute treatment with vehicle PBS, 80ng/mL CXCL12-WT, CXCL12-LM, or CXCL12-LD at 37°C. Following treatment, cells were fixed, permeabilized, and immunostained using a custom mouse monoclonal antibody specific for dually phosphorylated serine residues 324 and 325 (pSer324/325) (Clone 5E11), as described previously [78, 80]. Images were acquired using a Zeiss LSM 510 laser-scanning confocal microscope with a 63x W Apochromat oil-immersion objective. Image acquisition settings across parallel samples were identical.

Transwell Migration

Cells were passaged to 5 x 10^5 cells/mL the day prior to individual experiments. On the day of the experiment, cells were counted, washed twice, and plated to the upper well of a Transwell insert (Corning Incorporated, Corning, NY) at a density of 60,000 cells/well in assay

medium (RPMI-1640, 0.2% (w/v) BSA Fraction V (Thermo Fisher Scientific), with chemoattractants added to the bottom well in assay medium. Cell migration was measured after 2 hours. Transwell migration was enumerated by flow cytometry using the High Throughput Sampler attachment for the BD LSR-II flow cytometer. Results were analyzed with FlowJo software (BD Biosciences).

BRET Assays

HEK293T cells were passaged to 2 x 10^6 cells/mL the day prior to the experiment. On the day of the transfection, cell media was changed one hour prior to the introduction of the transfection mixture. OptiMEM was warmed to 37°C and 500 mL was aliquoted into a microfuge tube, along with 0.06 μg Receptor-CXCR4-RLuc8. 5 μg Venus-Transducer β-arrestin and MiniG, and 15.9 μL TransIT. The transfection mixture was incubated in the cell culture hood for 20 minutes and then added dropwise to the cell plates. Cells were then placed back into the incubator overnight.

The day of the BRET assay, cells were washed with PBS and trypsinized for 5 minutes. DMEM supplement with 10% (v/v) FBS was then added to neutralize the trypsin before cells were centrifuged for 5 minutes at 300 x g. Cells were then resuspended in PBS + 0.1% (v/v) glucose. A 15 μL aliquot of cells was placed into a microfuge tube and counted using hemocytometer. Cells should be at a final density of 100,000 cells/well of a 96-well plate. Cells were then plated into a 96-well plate and incubated for 1 hour. Next, the ligand plate was prepared, with the ligands of interest being CXCL12-WT, -LM, and –LD. Ligands were diluted in PBS + 0.1% (v/v) glucose to reach the desired final concentration of 30 μM. Serial dilutions of the ligands were then made in the 96-well plate. Coelenterazine H was resuspended to 1 mM using methanol, and a 50 μL working stock of Coelenterazine H into PBS + 0.1% (v/v) glucose buffer was made. 100 μL of this working stock was added to each well in row A of the 96-well

plate. 10 μL of the Coelenterazine H was then transferred from row A to the rest of the rows of the 96-well plate. The Omega plate reader (BMG Labtech; Cary, NC) was then used to measure bioluminescence. Net BRET was calculated using Excel.

Receptor Internalization

U937, THP-1, and AML-193 cells were counted and placed into 5mL polystyrene tubes at 10^6 cells/mL in 1.0 mL. Cells were treated with the denoted concentrations and variants of CXCL12 for the indicated times. After, the cells were washed twice with 0.5% (v/v) BSA in PBS. The cells then underwent a Fc receptor block (Biolegend, 422302) for 10 minutes, washed twice with 0.5% (v/v) BSA in PBS buffer, and then cell surface stained with either PE-conjugated CXCR4 antibody clone 12G5 (Invitrogen, 12-9999-42) or PE-conjugated clone 1D9 (BD, 551510) for 30 minutes. ACKR3 surface levels were measured using ACKR3-APC (Biolegend, 331114). After staining, the cells were washed twice with flow buffer and resuspended in 300-500 μL flow buffer. Surface CXCR4 and ACKR3 expression was quantified by analyzing the stained cell suspension on a Cytek Aurora spectral flow cytometer. AMD3100 was used at a concentration of 1 μM and BL-8040 was used at 100 nM. Results were analyzed with FlowJo software.

CXCL12-AzDye647 Imaging

2.5 x 10^5 U937 cells were grown on 24-well glass-bottom plates pre-coated with poly-D-lysine to enhance attachment. The cells were then treated with one of the following conditions: Vehicle-Control, 200 nM of CXCL12-WT-AzDye647, CXCL12-LM-AzDye647, or CXCL12-LD-AzDye647 for 30 minutes. After treatment, cells were counterstained with Hoechst nucleic acid stain to visualize nuclei and fixed with 4% (w/v) paraformaldehyde for 15 minutes. Imaging was performed using the Andor BC43 microscope (Oxford Instruments, Abingdon, UK) at 100X.

Images were analyzed using ImageJ and Amaris software. To quantify average fluorescence intensity per cell, the brightfield images of the cells were used to trace the cell border of all cells within the image. An area containing no cells was used to subtract background fluorescence from (**Supplemental Fig. 6**). The ImageJ EzColocalization plugin [81] was used to calculate the average red fluorescence intensity. The red channel only image was set as channel one with the cell-traced regions of interest set as the cell identifier. If multiple cells were within one image, the average fluorescence intensity per cell within that image was averaged before subtracting the background fluorescent intensity. The quantification shown represent an N of 2-3 with multiple 100X images taken per well with each dot representing the results from one image.

Bioinformatic Analysis

Analysis of a previously published dataset containing 16 AML patients and five healthy donors [45] was performed using the Seurat v5 (5.1.0) package in R version 4.4.1 [82]. The patient data was integrated using the Harmony package [83] Transcriptional regulon analysis was performed using the CollecTRI R package [53]. The volcano plot was generated using the EnhacedVolcano package. Single-cell RNA analysis of differentially expressed genes was performed using the MAST test [84]. The code for the analysis can be found at https://github.com/The-Michael-Dwinell-Lab-at-MCW/CXCL12-Locked-Dimer-AML. cBioPortal was used for gene correlations from The Cancer Genome Atlas. Specifically, the acute myeloid leukemia dataset was selected from the Pan-Cancer dataset with CXCR4 as the gene query.

Mice and Bone Marrow Cell Mobilization

All experiments were conducted under approved protocols from the Medical College of Wisconsin (AUA00076) and in accordance with the National Institutes of Health Guide for the Care and Use of Laboratory Animals and the ARRIVE guidelines [85]. Wildtype C57BL/6J were obtained from The Jackson Laboratory (Bar Harbor, ME). Animals were maintained on a strict

12:12 hour light–dark cycle in a temperature- and humidity-controlled facility with water and food provided ad libitum. Mice were injected with 200 μL 5 μM CXCL12-LD or 200 μL PBS subcutaneously in the right flank. Two hours after injection, mice were euthanized, and blood collected by cardiac puncture. Isolated blood was analyzed on the scil-Vet-abc Hematology Analyzer (scil Animal Care Company GmbH, Viernheim, Germany) to calculate the total number of monocytes per mm^3. In separate groups of mice, blood was collected from submandibular bleed 4 hours after injection with 200 μL 5 μM CXCL12-LD subcutaneously in the right flank. Red blood cells were lysed using manufacturers protocol (Biolegend 420301) and hematopoietic cells stained with Fixable viability dye eFluor 455 (BD Biosciences 65-0868-14), murine Fc block (Bio X Cell BE0307), murine anti-CD45 PerCP (ThermoFisher MA1-10234), murine anti-CXCR4 SuperBright 600 (ThermoFisher 63-9991-80), and/or murine anti-CD34 FITC (ThermoFisher 11-0341-82) and enumerated on a BD Fortessa flow cytometer (BD Biosciences, Franklin Lakes, NJ).

Ligand Transduction Coefficients and Bias Calculations

Raw values obtained from individual BRET experiments for both the G protein and β-arrestin recruitment were used to calculate a transduction ratio and bias relative to CXCL12-WT at each time point tested as previously described [84]. To calculate transduction coefficients, CXCL12-LM and CXLC12-LD values were normalized to CXCL12-LD. The Emax and EC_{50} values were calculated using the obtained normalized values. The values were then used to calculate the transduction ratio, or log of the relative activity using log RA = log(Emax/EC_{50}). The control-normalized factor was calculate using $\Delta\log RA = \log RA_{\text{CXCL12 isoform}} - \log RA_{\text{CXCL12-WT}}$. The log of the bias factor was calculated using $\Delta\Delta\log RA_{\text{CXCL12 isoform}} = \log RA_{\text{Pathway1}} - \log RA_{\text{Pathway2}}$. Lastly, the final bias factor was calculated using $10^{\Delta\Delta\log RA_{\text{CXCL12 isoform}}}$ [30].

Interalization in HeLa cells by ELISA

HeLa cells grown in 6-cm dishes were transiently transfected with CXCR4 (1 μg) tagged with FLAG and N-luc on the N- and C- terminus, respectively. The next day, 2 x 10^5 cells were seeded into a 24-well plate pre-coated for at least 1 hour with 0.1 mg/mL poly-L-lysine (Sigma; cat. No. P1399). Following overnight incubation at 37°C, cells were rinsed once with 500 μl of serum-free DMEM and treated with or without ligand for 30 minutes at 37°C. Cells were rinsed once with 500 μL ice-cold TBS buffer (20mM Tris, pH 7.5, 150mM NaCl) and immediately fixed for 5 minutes with 500 μL of 3.7% (v/v) formaldehyde diluted in TBS (Sigma; cat. No. F8775). Cells were washed three times with 500 μl TBS followed by incubation for 45 minutes at room temperature in TBS supplemented with 0.1% (w/v) bovine serum albumin (BSA) (Gold Bio cat. No. A-420-10). Thereafter, cells were incubated for 1 hour at room temperature with anti-FLAG M2 alkaline phosphatase-conjugated antibody diluted 1:3000 in TBS-BSA. Cells were washed 3 times with TBS and then incubated with a developing solution for 20 minutes when a light-yellow color was formed. Aliquots of each reaction were transferred to a 96-well plate containing 0.4 M of NaOH to quench the reaction. Absorbance readings were measured at 405 nm using a microplate reader. After background subtraction, receptor internalization was determined as a loss of surface receptor after ligand stimulation relative to the vehicle.

Statistical Analyses

Statistical analyses were performed using Prism 8.0 software (GraphPad Software, Irvine, CA). Power analysis was performed using an alpha error probability of 0.05 and a power level of 0.8 to select rigorous sample sizes for individual experiments. Unpaired sample comparisons between two groups were analyzed by Student's t-test when data was normally distributed with equal variances of the groups, or by Mann-Whitney test when parametric test conditions were violated. Three or more independent groups were compared using one-way or

two-way ANOVA with Dunnett's or Tukey's HSD test for multiple comparisons (test used denoted in figure legends).

ACKNOWLEDGMENTS

We thank Galina Petrova, PhD for expert guidance and training in the Children's Research Institute Flow Cytometry Shared Resource. We gratefully thank Megan C. Harwig, PhD, Microscopy Core Manager, for her invaluable assistance in completing the immunofluorescence microscopy.

Author contributions:

Author Contributions (CRediT Roles):

Conceptualization: MH, EC, DD, MBD

Data curation: MH, DM, DD

Formal Analysis: DD, MH, EC, DD

Funding acquisition: MBD

Investigation: DD, MH, EC, DM, AM, MP, ME

Methodology: DD, MP, MH, AM, MBD,

Project Administration: MBD

Resources: AM, FP, MBD

Software: AM

Supervision: MBD

Validation: MH, DM

Visualization: DD, MH, MP

Writing – original draft: MH

Writing – review and editing: DD, MH, EC, FP, AM, MBD

DATA AVAILABILITY

This study did not generate new unique reagents. All data are contained within the manuscript.

Grant support: This work is supported in part by grants from the National Cancer Institute R01 CA226279 to M.B.D and philanthropic support from the Hanis-Stepka-Rettig Endowed Chair in Cancer Research, and the Bobbie Nick Voss Charitable Foundation. The content is solely the responsibility of the author(s) and does not necessarily represent the official views of the NIH. D.D. is a member of the Medical Scientist Training Program at the Medical College of Wisconsin, which is supported in part by National Institutes of Health Training Grant T32 GM080202 from the National Institute of General Medical Sciences. D.D is supported in part by the grant from the National Cancer Institute F30 CA291095. The content is solely the responsibility of the author(s) and does not necessarily represent the official views of the National Institutes of Health.

Disclosures:

MBD and FP have financial interests in Protein Foundry, LLC and Xlock Biosciences, Inc. The remaining authors have no conflicts to disclose.

REFERENCES

1) Veldkamp, C. T., Peterson, F. C., Pelzek, A. J. & Volkman, B. F. The monomer-dimer equilibrium of stromal cell-derived factor-1 (CXCL 12) is altered by pH, phosphate, sulfate, and heparin. Protein Sci 14, 1071-1081, doi:10.1110/ps.041219505 (2005).
2) Veldkamp, C. T. et al. Structural basis of CXCR4 sulfotyrosine recognition by the chemokine SDF-1/CXCL12. Sci Signal 1, ra4, doi:10.1126/scisignal.1160755 (2008).
3) Ziarek, J. J. et al. Sulfopeptide probes of the CXCR4/CXCL12 interface reveal oligomer-specific contacts and chemokine allostery. ACS Chem Biol 8, 1955-1963, doi:10.1021/cb400274z (2013).
4) Roy, I. et al. Pancreatic Cancer Cell Migration and Metastasis Is Regulated by Chemokine-Biased Agonism and Bioenergetic Signaling. Cancer Res 75, 3529-3542, doi:10.1158/0008-5472.CAN-14-2645 (2015).
5) Roy, I., Getschman, A. E., Volkman, B. F. & Dwinell, M. B. Exploiting agonist biased signaling of chemokines to target cancer. Mol Carcinog 56, 804-813, doi:10.1002/mc.22571 (2017).
6) Guo, F. et al. CXCL12/CXCR4: a symbiotic bridge linking cancer cells and their stromal neighbors in oncogenic communication networks. Oncogene 35, 816-826, doi:10.1038/onc.2015.139 (2016).
7) Samarendra, H. et al. A meta-analysis of CXCL12 expression for cancer prognosis. Br J Cancer 117, 124-135, doi:10.1038/bjc.2017.134 (2017).
8) Ladikou, E. E., Chevassut, T., Pepper, C. J. & Pepper, A. G. Dissecting the role of the CXCL12/CXCR4 axis in acute myeloid leukaemia. Br J Haematol 189, 815-825, doi:10.1111/bjh.16456 (2020).
9) Roy, I. et al. Pancreatic Cancer Cell Migration and Metastasis Is Regulated by Chemokine-Biased Agonism and Bioenergetic Signaling. Cancer Res 75, 3529-3542, doi:10.1158/0008-5472.CAN-14-2645 (2015).
10) Drury, L. J. et al. Monomeric and dimeric CXCL12 inhibit metastasis through distinct CXCR4 interactions and signaling pathways. Proc Natl Acad Sci U S A 108, 17655-17660, doi:10.1073/pnas.1101133108 (2011).
11) Ziarek, J. J. et al. Structural basis for chemokine recognition by a G protein-coupled receptor and implications for receptor activation. Sci Signal 10, doi:10.1126/scisignal.aah5756 (2017).
12) Zhang, T. Y. et al. IL-6 blockade reverses bone marrow failure induced by human acute myeloid leukemia. Sci Transl Med 12, doi:10.1126/scitranslmed.aax5104 (2020).
13) Stubbins, R. J., Francis, A., Kuchenbauer, F. & Sanford, D. Management of Acute Myeloid Leukemia: A Review for General Practitioners in Oncology. Curr Oncol 29, 6245-6259, doi:10.3390/curroncol29090491 (2022).
14) Recher, C. et al. Long-term survival after intensive chemotherapy or hypomethylating agents in AML patients aged 70 years and older: a large patient data set study from European registries. Leukemia 36, 913-922, doi:10.1038/s41375-021-01425-9 (2022).
15) Appelbaum, F. R. et al. Age and acute myeloid leukemia. Blood 107, 3481-3485, doi:10.1182/blood-2005-09-3724 (2006).
16) Cho, B. S., Kim, H. J. & Konopleva, M. Targeting the CXCL12/CXCR4 axis in acute myeloid leukemia: from bench to bedside. Korean J Intern Med 32, 248-257, doi:10.3904/kjim.2016.244 (2017).
17) Sison, E. A., McIntyre, E., Magoon, D. & Brown, P. Dynamic chemotherapy-induced upregulation of CXCR4 expression: a mechanism of therapeutic resistance in pediatric AML. Mol Cancer Res 11, 1004-1016, doi:10.1158/1541-7786.MCR-13-0114 (2013).
18) Ding, L. et al. Clonal evolution in relapsed acute myeloid leukaemia revealed by whole-genome sequencing. Nature 481, 506-510, doi:10.1038/nature10738 (2012).

19) Nervi, B. et al. Chemosensitization of acute myeloid leukemia (AML) following mobilization by the CXCR4 antagonist AMD3100. Blood 113, 6206-6214, doi:10.1182/blood-2008-06-162123 (2009).
20) Cho, B. S. et al. Antileukemia activity of the novel peptidic CXCR4 antagonist LY2510924 as monotherapy and in combination with chemotherapy. Blood 126, 222-232, doi:10.1182/blood-2015-02-628677 (2015).
21) Zhang, Y. et al. CXCR4 inhibitors selectively eliminate CXCR4-expressing human acute myeloid leukemia cells in NOG mouse model. Cell Death Dis 3, e396, doi:10.1038/cddis.2012.137 (2012).
22) Abraham, M. et al. The CXCR4 inhibitor BL-8040 induces the apoptosis of AML blasts by downregulating ERK, BCL-2, MCL-1 and cyclin-D1 via altered miR-15a/16-1 expression. Leukemia 31, 2336-2346, doi:10.1038/leu.2017.82 (2017).
23) Roboz, G. J. et al. Phase I trial of plerixafor combined with decitabine in newly diagnosed older patients with acute myeloid leukemia. Haematologica 103, 1308-1316, doi:10.3324/haematol.2017.183418 (2018).
24) Martinez-Cuadron, D. et al. A phase I-II study of plerixafor in combination with fludarabine, idarubicin, cytarabine, and G-CSF (PLERIFLAG regimen) for the treatment of patients with the first early-relapsed or refractory acute myeloid leukemia. Ann Hematol 97, 763-772, doi:10.1007/s00277-018-3229-5 (2018).
25) Uy, G. L. et al. A phase 1/2 study of chemosensitization with the CXCR4 antagonist plerixafor in relapsed or refractory acute myeloid leukemia. Blood 119, 3917-3924, doi:10.1182/blood-2011-10-383406 (2012).
26) Uy, G. L. et al. A phase 1/2 study of chemosensitization with plerixafor plus G-CSF in relapsed or refractory acute myeloid leukemia. Blood Cancer J 7, e542, doi:10.1038/bcj.2017.21 (2017).
27) Segura, S. J. et al. Double-blind placebo controlled, randomized, multicenter, phase II study to assess the efficacy of the high affinity CXCR4 inhibitor BL-8040 as addition to consolidation therapy in AML by the SAL and OSHO leukemia study groups. Blood 140, 3338-3340, doi:10.1182/blood-2022-166748 (2022).
28) Li, X. et al. A designed peptide targeting CXCR4 displays anti-acute myelocytic leukemia activity in vitro and in vivo. Sci Rep 4, 6610, doi:10.1038/srep06610 (2014).
29) Crump, M. P. et al. Solution structure and basis for functional activity of stromal cell-derived factor-1; dissociation of CXCR4 activation from binding and inhibition of HIV-1. EMBO J 16, 6996-7007, doi:10.1093/emboj/16.23.6996 (1997).
30) Caroli, J. et al. A community Biased Signaling Atlas. Nat Chem Biol 19, 531-535, doi:10.1038/s41589-023-01292-8 (2023).
31) Busillo, J. M. et al. Site-specific phosphorylation of CXCR4 is dynamically regulated by multiple kinases and results in differential modulation of CXCR4 signaling. J Biol Chem 285, 7805-7817, doi:10.1074/jbc.M109.091173 (2010).
32) Moo, E. V., van Senten, J. R., Brauner-Osborne, H. & Moller, T. C. Arrestin-Dependent and -Independent Internalization of G Protein-Coupled Receptors: Methods, Mechanisms, and Implications on Cell Signaling. Mol Pharmacol 99, 242-255, doi:10.1124/molpharm.120.000192 (2021).
33) Busillo, J. M. & Benovic, J. L. Regulation of CXCR4 signaling. Biochim Biophys Acta 1768, 952-963, doi:10.1016/j.bbamem.2006.11.002 (2007).
34) Abraham, M. et al. Single Dose of the CXCR4 Antagonist BL-8040 Induces Rapid Mobilization for the Collection of Human CD34(+) Cells in Healthy Volunteers. Clin Cancer Res 23, 6790-6801, doi:10.1158/1078-0432.CCR-16-2919 (2017).
35) Hatse, S., Princen, K., Bridger, G., De Clercq, E. & Schols, D. Chemokine receptor inhibition by AMD3100 is strictly confined to CXCR4. FEBS Lett 527, 255-262, doi:10.1016/s0014-5793(02)03143-5 (2002).

36) Carnec, X., Quan, L., Olson, W. C., Hazan, U. & Dragic, T. Anti-CXCR4 monoclonal antibodies recognizing overlapping epitopes differ significantly in their ability to inhibit entry of human immunodeficiency virus type 1. J Virol 79, 1930-1933, doi:10.1128/JVI.79.3.1930-1933.2005 (2005).
37) Kaiser, L. M. et al. Targeting of CXCR4 by the Naturally Occurring CXCR4 Antagonist EPI-X4 in Waldenstrom's Macroglobulinemia. Cancers (Basel) 13, doi:10.3390/cancers13040826 (2021).
38) Bachelerie, F. et al. International Union of Basic and Clinical Pharmacology. [corrected]. LXXXIX. Update on the extended family of chemokine receptors and introducing a new nomenclature for atypical chemokine receptors. Pharmacol Rev 66, 1-79, doi:10.1124/pr.113.007724 (2014).
39) Meyrath, M. et al. The atypical chemokine receptor ACKR3/CXCR7 is a broad-spectrum scavenger for opioid peptides. Nat Commun 11, 3033, doi:10.1038/s41467-020-16664-0 (2020).
40) Hess, E. J., Norman, A. B. & Creese, I. Chronic treatment with dopamine receptor antagonists: behavioral and pharmacologic effects on D1 and D2 dopamine receptors. J Neurosci 8, 2361-2370, doi:10.1523/JNEUROSCI.08-07-02361.1988 (1988).
41) Smit, M. J. et al. Inverse agonism of histamine H2 antagonist accounts for upregulation of spontaneously active histamine H2 receptors. Proc Natl Acad Sci U S A 93, 6802-6807, doi:10.1073/pnas.93.13.6802 (1996).
42) von Zastrow, M. & Kobilka, B. K. Antagonist-dependent and -independent steps in the mechanism of adrenergic receptor internalization. J Biol Chem 269, 18448-18452 (1994).
43) Sison, E. A. et al. Plerixafor as a chemosensitizing agent in pediatric acute lymphoblastic leukemia: efficacy and potential mechanisms of resistance to CXCR4 inhibition. Oncotarget 5, 8947-8958, doi:10.18632/oncotarget.2407 (2014).
44) Bouaboula, M., Dussossoy, D. & Casellas, P. Regulation of peripheral cannabinoid receptor CB2 phosphorylation by the inverse agonist SR 144528. Implications for receptor biological responses. J Biol Chem 274, 20397-20405, doi:10.1074/jbc.274.29.20397 (1999).
45) Broxmeyer, H. E. et al. Rapid mobilization of murine and human hematopoietic stem and progenitor cells with AMD3100, a CXCR4 antagonist. J Exp Med 201, 1307-1318, doi:10.1084/jem.20041385 (2005).
46) van Galen, P. et al. Single-Cell RNA-Seq Reveals AML Hierarchies Relevant to Disease Progression and Immunity. Cell 176, 1265-1281 e1224, doi:10.1016/j.cell.2019.01.031 (2019).
47) Zhou, C. et al. JUN is a key transcriptional regulator of the unfolded protein response in acute myeloid leukemia. Leukemia 31, 1196-1205, doi:10.1038/leu.2016.329 (2017).
48) Korthuis, P. M. et al. CITED2-mediated human hematopoietic stem cell maintenance is critical for acute myeloid leukemia. Leukemia 29, 625-635, doi:10.1038/leu.2014.259 (2015).
49) Mattes, K., Berger, G., Geugien, M., Vellenga, E. & Schepers, H. CITED2 affects leukemic cell survival by interfering with p53 activation. Cell Death Dis 8, e3132, doi:10.1038/cddis.2017.548 (2017).
50) Kawahara, M. et al. H2.0-like homeobox (HLX) regulates early hematopoiesis and promotes acute myeloid leukemia. Cancer Cell, 22(2), 194-208, doi: 10.1016/j.ccr.2012.06.027 (2013).
51) Piragyte, I. et al. A metabolic interplay coordinate by HLX regulate myeloid differentiation and AML through partly overlapping pathways. Nat Commun, 9(1) 3090. doi: 10.1038/s41467-018-05311-4 (2018).

52) Hu, CL. Et al. Targeting UHRF1-SAP30-MXD4 axis for leukemia initiating cell eradication in myeloid leukemia. Cell Res, 32(12), 1105-1123. doi: 10.1038/s41422-022-00735-6 (2022).
53) Pokhilko, A. et al. Targeted single-cell RNA sequencing of transcription factors enhance the identification of cell types and trajectories. Genome Res, 31(6), 1069-1081. doi: 10.1101/gr.273961.120 (2021).
54) Muller-Dott, S. et al. Expanding the coverage of regulons from high-confidence prior knowledge for accurate estimation of transcription factor activities. Nucleic Acids Res 51, 10934-10949, doi:10.1093/nar/gkad841 (2023).
55) Takeda, R. et al. HHEX promotes myeloid transformation in cooperation with mutant ASXL1. Blood 136, 1670-1684, doi:10.1182/blood.2019004613 (2020).
56) Loizou, E. et al. A Gain-of-Function p53-Mutant Oncogene Promotes Cell Fate Plasticity and Myeloid Leukemia through the Pluripotency Factor FOXH1. Cancer Discov 9, 962-979, doi:10.1158/2159-8290.CD-18-1391 (2019).
57) Zhang, W. B. et al. A point mutation that confers constitutive activity to CXCR4 reveals that T140 is an inverse agonist and that AMD3100 and ALX40-4C are weak partial agonists. J Biol Chem 277, 24515-24521, doi:10.1074/jbc.M200889200 (2002).
58) Rebolledo-Bustillo, M. et al. Structural Basis of the Binding Mode of the Antineoplastic Compound Motixafortide (BL-8040) in the CXCR4 Chemokine Receptor. Int J Mol Sci 24, doi:10.3390/ijms24054393 (2023).
59) Kufareva, I., Gustavsson, M., Zheng, Y., Stephens, B. S. & Handel, T. M. What Do Structures Tell Us About Chemokine Receptor Function and Antagonism? Annu Rev Biophys 46, 175-198, doi:10.1146/annurev-biophys-051013-022942 (2017).
60) Stephens, B. S., Ngo, T., Kufareva, I. & Handel, T. M. Functional anatomy of the full-length CXCR4-CXCL12 complex systematically dissected by quantitative model-guided mutagenesis. Sci Signal 13, doi:10.1126/scisignal.aay5024 (2020).
61) Trent, J. O. et al. Lipid bilayer simulations of CXCR4 with inverse agonists and weak partial agonists. J Biol Chem 278, 47136-47144, doi:10.1074/jbc.M307850200 (2003).
62) Vales, S. et al. Discovery and pharmacophoric characterization of chemokine network inhibitors using phage-display, saturation mutagenesis and computational modelling. Nat Commun 14, 5763, doi:10.1038/s41467-023-41488-z (2023).
63) Seibert, C. et al. Sequential tyrosine sulfation of CXCR4 by tyrosylprotein sulfotransferases. Biochemistry 47, 11251-11262, doi:10.1021/bi800965m (2008).
64) Marchese, A., Paing, M.M., Temple, B.R.S. & Trejo, A. G-protein coupled receptor sorting to endosomes and lysosomes. Annu Rev Pharmacol Toxicol 48, 601-629, doi: 10.1146/annurev.pharmtox.48.113006.094646 (2008).
65) Robleto, V.R., Zhuo, Y., Crecelius, J.M., Benzow, S. & Marchese, A. SNX9 family mediates Barrestin-independent GPCR endocytosis. Commun Biol 7(1), 1455. doi: 10.1038/s42003-024-07157-7 (2024).
66) Zeng, Z. et al. Targeting the leukemia microenvironment by CXCR4 inhibition overcomes resistance to kinase inhibitors and chemotherapy in AML. Blood 113, 6215-6224, doi:10.1182/blood-2008-05-158311 (2009).
67) Borthakur, G. et al. BL-8040 CXCR4 antagonist is safe and demonstrates antileukemic activity in combination with cytarabine for the treatment of relapsed/refractory acute myelogenous leukemia: An open-label safety and efficacy phase 2a study. Cancer 127, 1246-1259, doi:10.1002/cncr.33338 (2021).
68) Boddu, P. et al. Initial Report of a Phase I Study of LY2510924, Idarubicin, and Cytarabine in Relapsed/Refractory Acute Myeloid Leukemia. Front Oncol 8, 369, doi:10.3389/fonc.2018.00369 (2018).

69) Van Hout, A., D'Huys, T., Oeyen, M., Schols, D. & Van Loy, T. Comparison of cell-based assays for the identification and evaluation of competitive CXCR4 inhibitors. PLoS One 12, e0176057, doi:10.1371/journal.pone.0176057 (2017).
70) Grudzien, P., Neufeld, H., Ebe Eyenga, M. & Gaponenko, V. Development of tolerance to chemokine receptor antagonists: current paradigms and the need for further investigation. Front Immunol 14, 1184014, doi:10.3389/fimmu.2023.1184014 (2023).
71) Hitchinson, B. et al. Biased antagonism of CXCR4 avoids antagonist tolerance. Sci Signal 11, doi:10.1126/scisignal.aat2214 (2018).
72) Malik, R. & Marchese, A. Arrestin-2 interacts with the endosomal sorting complex required for transport machinery to modulate endosomal sorting of CXCR4. Mol Biol Cell 21, 2529-2541, doi:10.1091/mbc.e10-02-0169 (2010).
73) Zhuo, Y., Crecelius, J.M. & Marchese, A. G protein-coupled receptor kinase phosphorylation of distal C-tail sites specifies Barrestin1-mediated signaling by chemokine receptor CXCR4. J Biol Chem 298(9), 102351, doi: 10.1016/j.jbc.2022.102351 (2022).
74) Ziarek, J. J. et al. Heparin oligosaccharides inhibit chemokine (CXC motif) ligand 12 (CXCL12) cardioprotection by binding orthogonal to the dimerization interface, promoting oligomerization, and competing with the chemokine (CXC motif) receptor 4 (CXCR4) N terminus. J Biol Chem 288, 737-746, doi:10.1074/jbc.M112.394064 (2013).
75) Antos, J. M., Truttmann, M. C. & Ploegh, H. L. Recent advances in sortase-catalyzed ligation methodology. Curr Opin Struct Biol 38, 111-118, doi:10.1016/j.sbi.2016.05.021 (2016).
76) Gutjahr, J. C. et al. The dimeric form of CXCL12 binds to atypical chemokine receptor 1. Sci Signal 14, doi:10.1126/scisignal.abc9012 (2021).
77) Dwinell, M. B., Ogawa, H., Barrett, K. E. & Kagnoff, M. F. SDF-1/CXCL12 regulates cAMP production and ion transport in intestinal epithelial cells via CXCR4. Am J Physiol Gastrointest Liver Physiol 286, G844-850, doi:10.1152/ajpgi.00112.2003 (2004).
78) Bhandari, D., Robia, S. L. & Marchese, A. The E3 ubiquitin ligase atrophin interacting protein 4 binds directly to the chemokine receptor CXCR4 via a novel WW domain-mediated interaction. Mol Biol Cell 20, 1324-1339, doi:10.1091/mbc.e08-03-0308 (2009).
79) Marchese, A. Monitoring Chemokine Receptor Trafficking by Confocal Immunofluorescence Microscopy. Methods Enzymol 570, 281-292, doi:10.1016/bs.mie.2015.10.004 (2016).
80) Caballero, A., Mahn, S. A., Ali, M. S., Rogers, M. R. & Marchese, A. Heterologous regulation of CXCR4 lysosomal trafficking. J Biol Chem 294, 8023-8036, doi:10.1074/jbc.RA118.005991 (2019).
81) Stauffer, W., Sheng, H. & Kim, H.N. EzColocalization: An ImageJ plugin for visualizing and measuring colocalization in cells and organisms. Sci Rep 8(1), 15764, doi: 10.1038/s41598-018-33592-8 (2018).
82) Hao, Y. et al. Integrated analysis of multimodal single-cell data. Cell 184, 3573-3587 e3529, doi:10.1016/j.cell.2021.04.048 (2021).
83) Korsunsky, I. et al. Fast, sensitive and accurate integration of single-cell data with Harmony. Nat Methods 16, 1289-1296, doi:10.1038/s41592-019-0619-0 (2019).
84) Finak, M. et al. MAST: a flexible statistical framework for assessing transcriptional changes and characterizing heterogeneity in single-cell RNA sequencing data. Genome Biol 10, 278. doi: 10.1186/s13059-015-0844-5 (2015).
85) Percie du Sert, N. et al. Reporting animal research: Explanation and elaboration for the ARRIVE guidelines 2.0. PLoS Biol 18, e3000411, doi:10.1371/journal.pbio.3000411 (2020).

Figure Legends

Figure 1: CXCR4 expression in AML cell lines. (A) RT-PCR of CXCR4, ACKR3, and beta actin in three human AML cell lines U937, THP-1, and AML-193. Data representative of 3 separate analyses. **(B)** Flow cytometry results of the three AML cell lines stained with either anti-CXCR4 clone 12G5 or control isotype antibody. * = $P \leq 0.05$ by Student's t-test. n = 2-3 independent analyses. Values are mean ± SEM. **(C)** U937 or **(D)** THP-1 cell chemotaxis from the top chamber of a transwell filter towards the lower chamber containing the indicated concentration of CXCL12-WT chemokine. All values under significance bar represent a significant increase by one-way ANOVA with Dunnett's multiple comparison test to 0 nM vehicle treated. **(E)** Total number of U937 or **(F)** THP-1 migrated from the top chamber of a transwell chamber towards the lower chamber containing the indicated concentration of CXCL12-WT, CXCL12-LM, or CXCL12-LD. Migrating cells in panels C-F were enumerated after a two hour incubation using flow cytometry. Values represent mean ± SEM, n = 3-4 independent biological replicates. Red asterisks or numbers indicate adjusted p value by two-way ANOVA with Tukey's multiple comparisons test to that respective variant's 0 nM (*e.g.* CXCL12-WT 30 nM to CXCL12-WT 0 nM) while blue indicates significance compared to the same dose of a different variant (*e.g.* CXCL12-LD 30nM to CXCL12-WT 30nM).

Figure 2: CXCL12-LD is a balanced partial agonist. (A) cAMP levels in THP-1 cells stimulated with 10 mM IBMX and 1 μM forskolin followed by treatment with various compounds measured by a competitive enzyme immunoassay. All significance values are in relation to FSK/IBMX by two-way ANOVA with Dunnett's multiple comparison test. **(B, C)** Calcium flux in THP-1 and U937 cells treated with either CXCL12-WT or CXCL12-LD. n = 3. **(D)** AML cells were pre-treated with pertussis toxin prior to treatment with CXCL12 variants. All pertussis toxin pre-treated values are significantly different by Student's t-test when compared to the same form of CXCL12 without pertussis toxin. **(E)** The $\log(E_{max}/EC_{50})$ of the CXCL12 variants from net BRET in HEK293-CXCR4-Luc cells transfected with β-arrestin or Gαi Venus transducer. n = 6, EC_{50} values calculated from non-linear curve fit, all r^2 values > 0.82. **(F)** Bias factors for CXCL12-WT, -LM, and -LD at all timepoints tested from HEK293 BRET studies calculated using the calculator found on the Biased Signaling Atlas [30]. A bias factor >5 is indicative of biased agonism.

Figure 3: Differential CXCR4 C-terminal phosphorylation in response to CXCL12 variants. (A) HeLa cells transiently transfected with HA-CXCR4-YFP were stimulated with vehicle, **(B)** CXCL12-WT, **(C)** CXCL12-LM, or **(D)** CXCL12-LD. The far left panels show visualization of YFP-CXCR4 and the middle left panel is visualization of the phosphorylated Ser324/325 residues on CXCR4. Co-localization of the YFP-CXCR4 and phosphorylated CXCR4 appear yellow in the merge panel on the middle right. Differential image contrast (DIC) images are shown on the far right panels. Shown are the representative micrographs from three independent experiments. Bars = 20 μm.

Figure 4: CXCL12-LD promotes internalization of CXCR4. **(A)** Percent of CXCR4 positive U937 cells detected by flow cytometry with the 12G5 CXCR4 antibody after 30 minutes or **(B)** 24 hours of incubation with various concentrations of CXCL12 WT (blue), LM (orange), or LD (green). * represent significance when comparing to vehicle and # represents significance when comparing to respective dose of CXCL12-WT (*e.g.* CXCL12-LD 10 nM to CXCL12-WT), adjusted $P \leq 0.05$ by two-way ANOVA with Tukey's multiple comparison test. **(C)** The percent of CXCR4 positive U937 cells detected by flow cytometry with the 1D9 CXCR4 antibody after 30 minutes or **(D)** 24 hours of incubation with various concentrations of CXCL12 variants. **(E)** Three

different leukimic cell lines treated with CXCL12 WT, LM, or LD and stained with the 1D9 antibody after 30 minutes of treatment or **(F)** 24 hours. Significance represents comparison of CXCL12-variant to CXCL12-WT in the same cell line by one-way ANOVA with Dunnett's multiple comparison test, $P \leq 0.05$.

Figure 5: Labeled CXCL12 ligands show internalization with CXCL12-LD. (A) U937 cells were treated with 200 nM of AzDye647-conjugated CXCL12 variants (red, bottom right of one image) of their respective variant for 30 minutes before fixation and staining with Hoechst 3342 (cyan, bottom left). Brightfield is shown in the top right and the merged image is the top left. Images shown are at 100X. Scale bar is 50 μm. **(B)** Enhancement on the cutout of the images in the white square from Fig. 5A. **(C)** Untreated U937 cells shown under the same conditions as figure 5A and 5B. **(D)** Quantification of the corrected (background substracted) average red AzDye647 fluorescence intensity inside of cells. Red asterisks indicate significance compared to control and blue asterisks indicate signficance compared to CXCL12-WT by one-way ANOVA with Tukey's multiple comparisons test, $P \leq 0.05$.

Figure 6: CXCR4 surface upregulation seen with AMD3100 and BL-8040 but not CXCL12-LD. (A) U937 cells were treated with either 1 μM AMD3100, 100 nM BL-8040, or 100 nM CXCL12-LD and immunostained for surface CXCR4 with the 1D9 clone. Mean fluorescent intensity (MFI) values were normalized against vehicle-treated (PBS) U937 cells stained for surface CXCR4. Treatment was for 30 minutes or **(B)** 24 hours. **(C)** CXCR4 inhibitor treatment of AML-293 cells for 30 minutes or **(D)** 24 hours under the same conditions seen in 6A and 6B. * = $P \leq 0.05$ by one-way ANOVA with Tukey's multiple comparisons test.

Figure 7: **CXCL12-LD increases the frequency of hematopoietic progenitor cells in peripheral blood. (A)** Dot plot of CXCR4 expression in the bone marrow aspirates of 16 AML patient's pre-treatment [46]. Each of the "-like" cells had a confirmed mutation in a targeted DNA sequence to confirm their malignancy. **(B)** The "Mono" and "Mono-like" cell types were further analyzed for CXCR4 expression. CXCR4 was elevated in the Mono-like (Malignant monocyte) compared to the Mono (Healthy monocyte) by MAST test ($P \leq 0.05$) [84]. **(C)** The malignant monocyte population from figure 6B was grouped by CXCR4 expression. Differentially expressed genes by MAST test were found and plotted on the volcano plot. Grey dots represent non-significant genes by both log2FC or adjusted p-value, green dots represent genes with significant adjusted p-value but not log2FC, blue dots represent genes with significant log2FC but not adjusted p-value, and red dots represent genes with both significant log2FC and adjusted p-value. Log2FC threshold was 0.5 and adjusted p-value threshold was 0.005. **(D)** The malignant monocytes sorted by CXCR4 expression were analyzed using the CollecTRI R package to estimate the transcription factor activity based on weighted mean gene expression with the obtained t-values of the slope plotted. Positive values represent inferred transcription factor activity while negative values represent inferred inactive transcription factor activity. **(E)** Wildtype C57BL/6 mice were given 200 μL 5 μM CXCL12-LD or vehicle PBS. The frequency of total monocytes **(E)** and CD34+ CXCR4+ progenitor cells **(F)** in peripheral blood was measured two hours after treatment. Values are mean ± SD from 3-6 separate mice.

Figure 8: CXCL12-LD functions differently than currently available CXCR4 inhibitors. **Left**, CXCL12 produced by bone marrow stromal cells maintains chemoresistant CXCR4-expressing AML blasts in the marrow. If CXCR4 expression is lost or the receptor is inhibited, the blasts are mobilized into the bloodstream. **Right**, 2nd generation CXCR4 inhibitors are shown to be inverse agonists of CXCR4 that inhibit internalization and result in surface receptor upregulation. In the middle, CXCL12-WT as a balanced agonist activating both β-arrestin and the G-protein

signaling pathways. Signaling with CXCL12-WT results in receptor internalization and recycling. On the right, CXCL12-LD is a partial agonist whose signaling results in greater receptor internalization compared to CXCL12-WT, possibly through increased receptor lysosomal degradation rather than endosomal recycling. Created in BioRender. Drouillard, D. (2025) https://BioRender.com/t28xc88.

Figure 1.

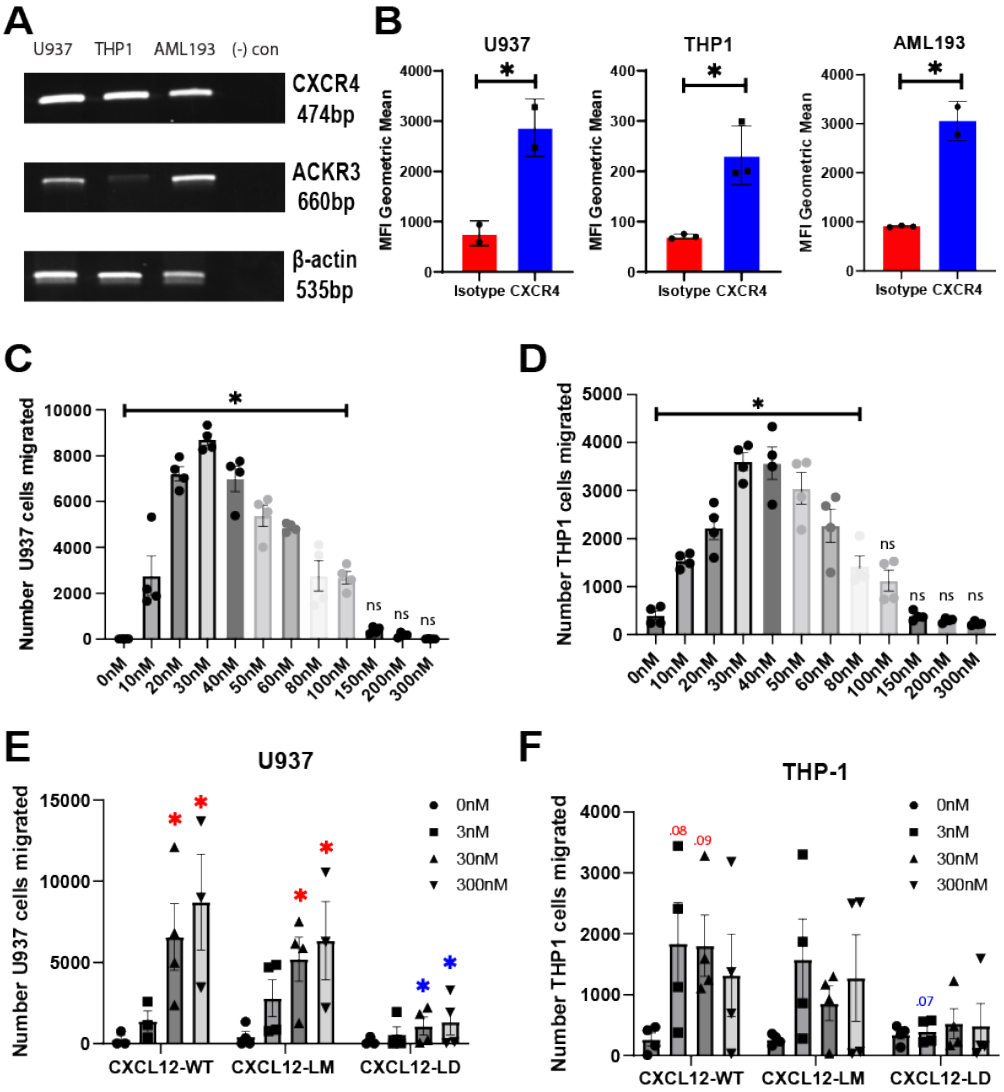
A
U937 THP1 AML193 (-) con
CXCR4 474bp
ACKR3 660bp
β-actin 535bp
B
U937
THP1
AML193
MFI Geometric Mean
Isotype CXCR4
C
Number U937 cells migrated
0nM 10nM 20nM 30nM 40nM 50nM 60nM 80nM 100nM 150nM 200nM 300nM
D
Number THP1 cells migrated
E
U937
Number U937 cells migrated
0nM
3nM
30nM
300nM
CXCL12-WT
CXCL12-LM
CXCL12-LD
F
THP-1
Number THP1 cells migrated

Figure 2.

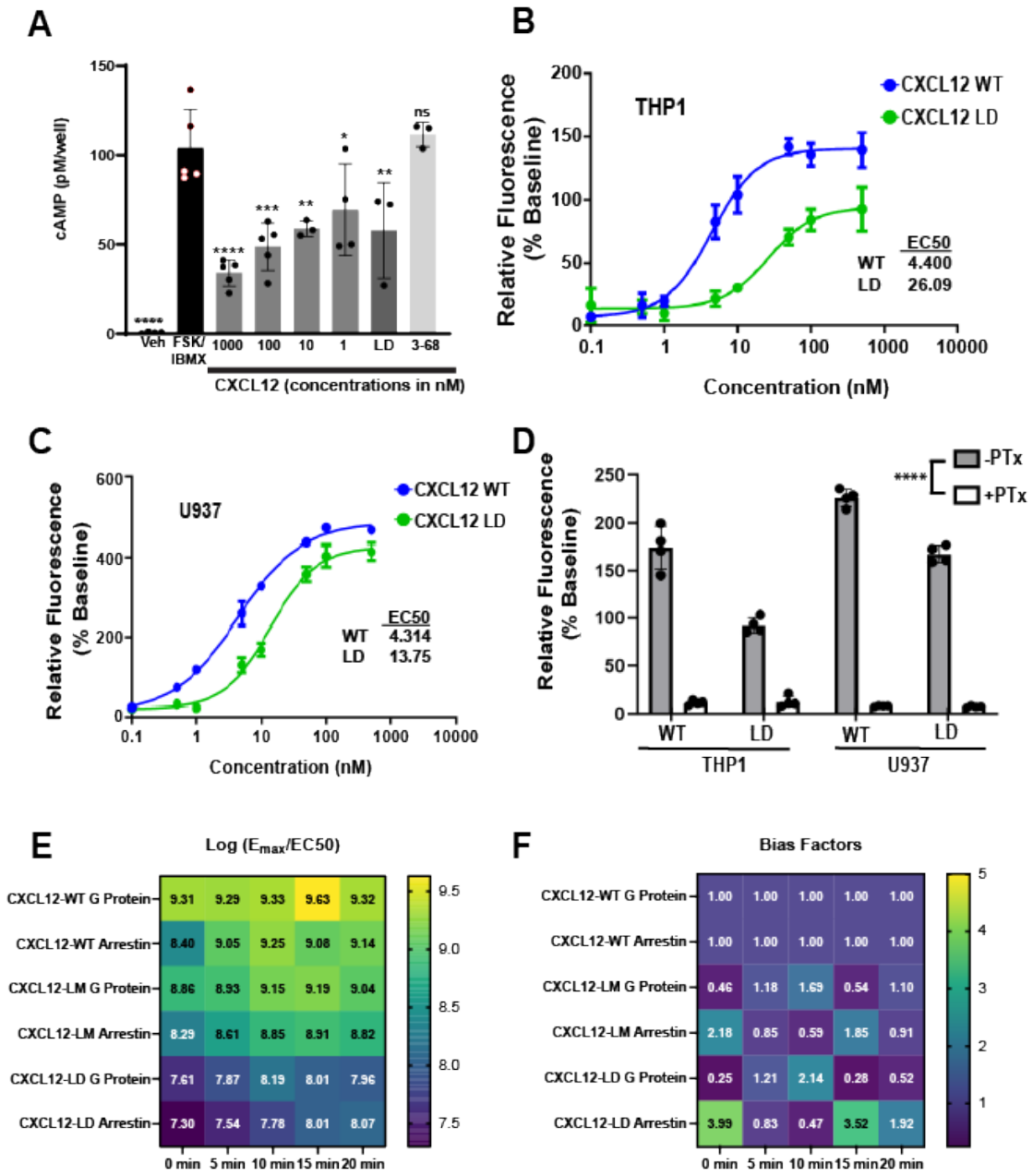
A
cAMP (pM/well)
Veh
FSK/ IBMX
1000
100
10
1
LD
3-68
CXCL12 (concentrations in nM)
ns
B
THP1
CXCL12 WT
CXCL12 LD
Relative Fluorescence (% Baseline)
EC50
WT 4.400
LD 26.09
Concentration (nM)
C
U937
CXCL12 WT
CXCL12 LD
EC50
WT 4.314
LD 13.75
Relative Fluorescence (% Baseline)
Concentration (nM)
D
-PTx
+PTx
Relative Fluorescence (% Baseline)
WT
LD
THP1
U937
E
Log (Emax/EC50)
CXCL12-WT G Protein 9.31 9.29 9.33 9.63 9.32
CXCL12-WT Arrestin 8.40 9.05 9.25 9.08 9.14
CXCL12-LM G Protein 8.86 8.93 9.15 9.19 9.04
CXCL12-LM Arrestin 8.29 8.61 8.85 8.91 8.82
CXCL12-LD G Protein 7.61 7.87 8.19 8.01 7.96
CXCL12-LD Arrestin 7.30 7.54 7.78 8.01 8.07
0 min 5 min 10 min 15 min 20 min
F
Bias Factors
CXCL12-WT G Protein 1.00 1.00 1.00 1.00 1.00
CXCL12-WT Arrestin 1.00 1.00 1.00 1.00 1.00
CXCL12-LM G Protein 0.46 1.18 1.69 0.54 1.10
CXCL12-LM Arrestin 2.18 0.85 0.59 1.85 0.91
CXCL12-LD G Protein 0.25 1.21 2.14 0.28 0.52
CXCL12-LD Arrestin 3.99 0.83 0.47 3.52 1.92
0 min 5 min 10 min 15 min 20 min

Figure 3.

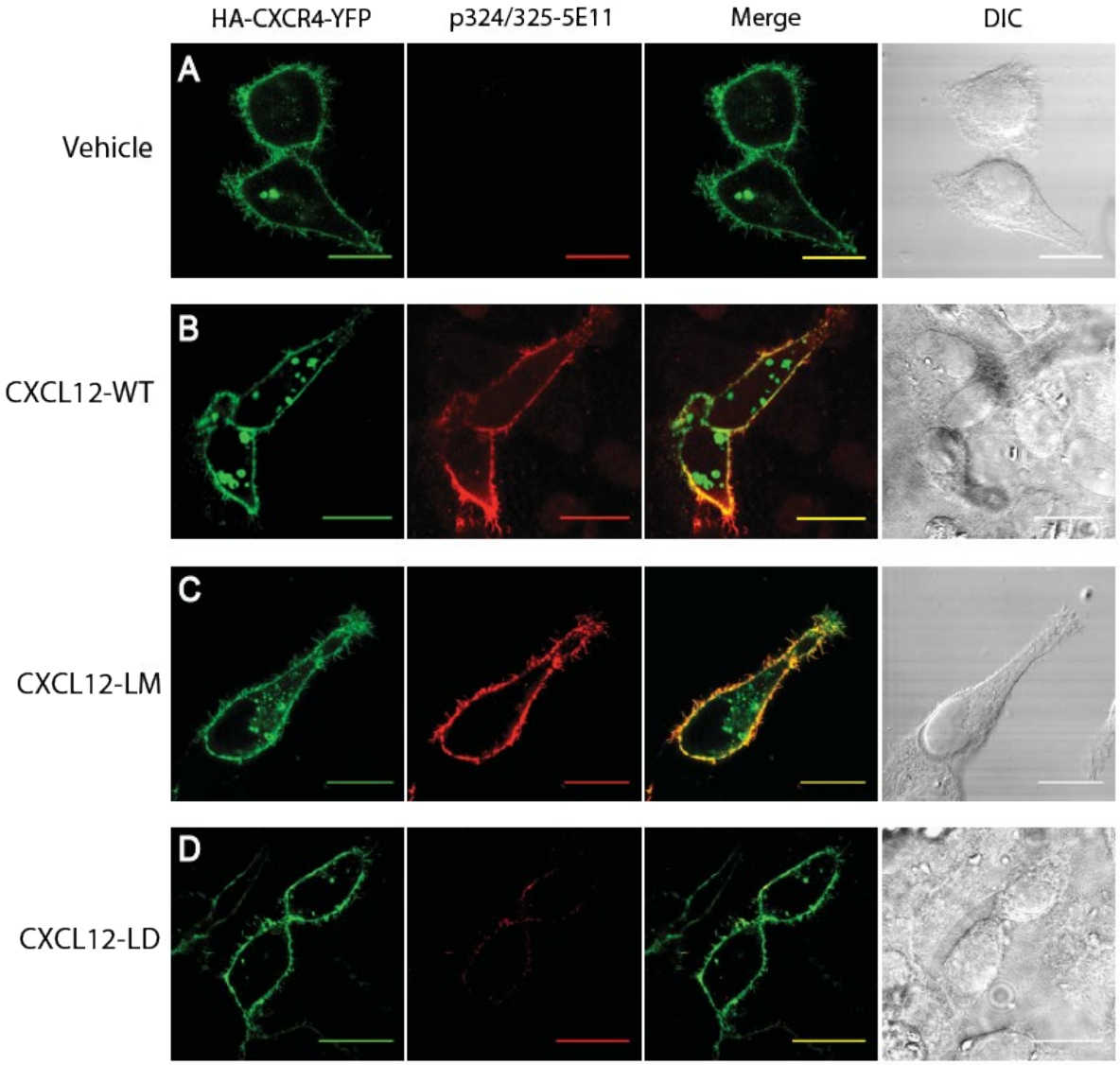
HA-CXCR4-YFP
p324/325-5E11
Merge
DIC
A
Vehicle
B
CXCL12-WT
C
CXCL12-LM
D
CXCL12-LD

Figure 4.

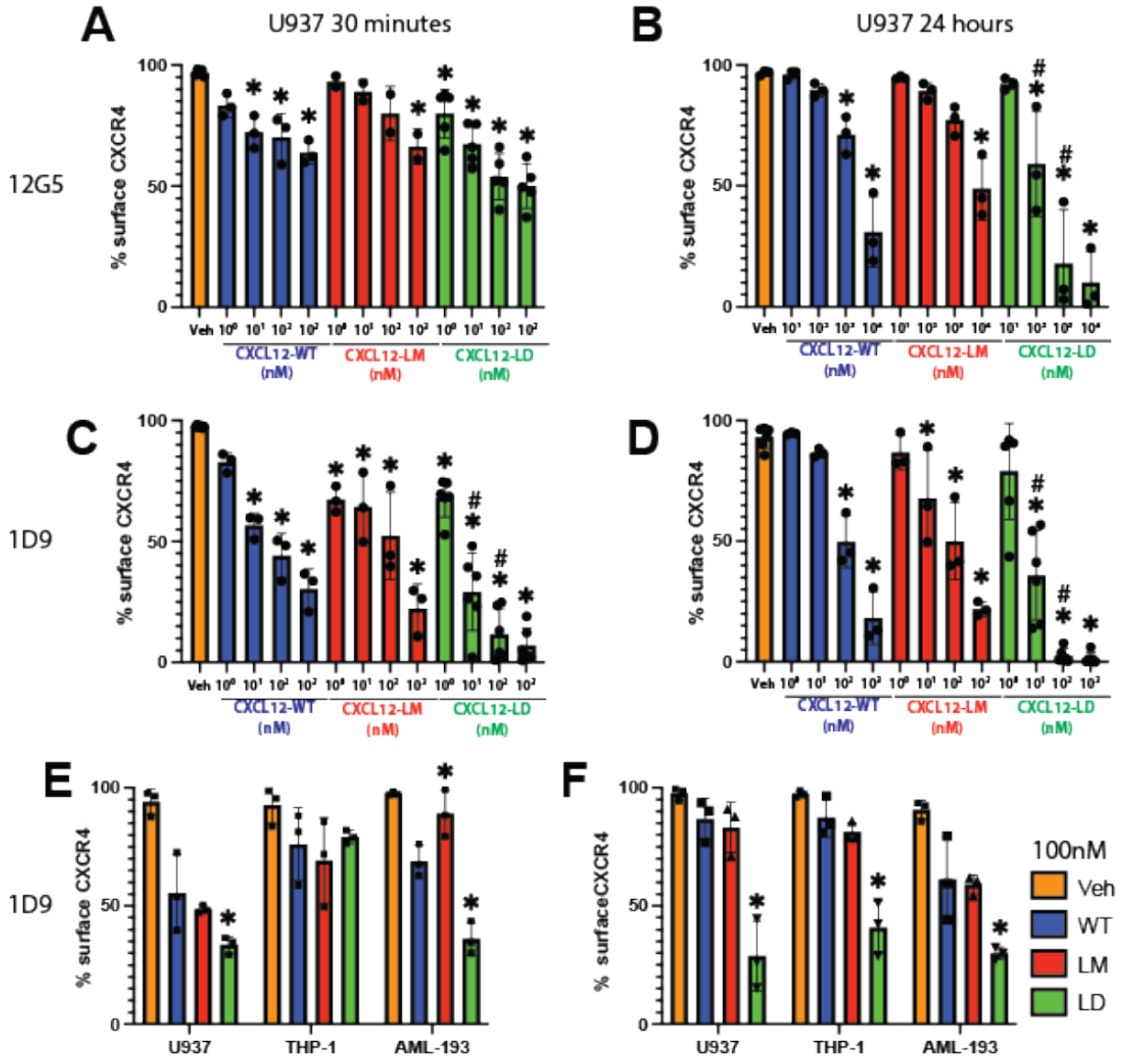
A
U937 30 minutes
B
U937 24 hours
12G5
% surface CXCR4
100
50
0
Veh
CXCL12-WT (nM)
CXCL12-LM (nM)
CXCL12-LD (nM)
C
D
1D9
E
F
U937
THP-1
AML-193
100nM
Veh
WT
LM
LD

Figure 5.

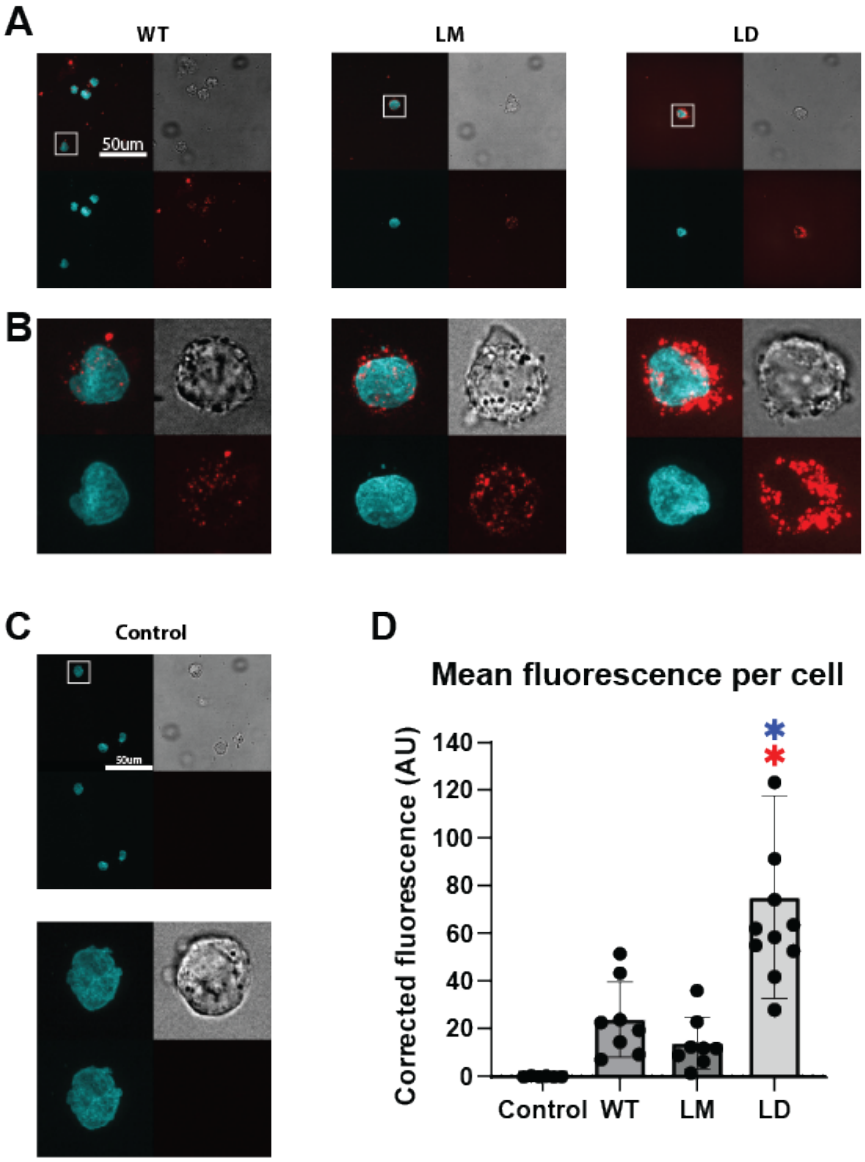
A
WT
LM
LD
50um
B
C
Control
50um
D
Mean fluorescence per cell
Corrected fluorescence (AU)
140
120
100
80
60
40
20
0
Control
WT
LM
LD

Figure 6.

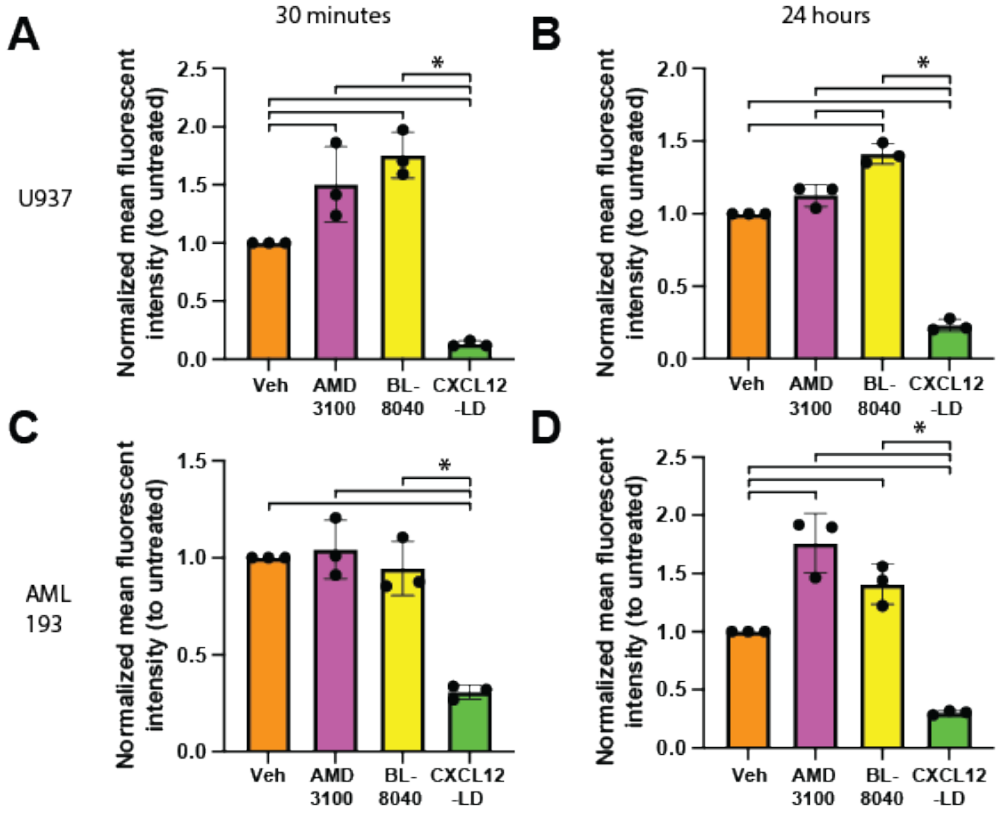
A
30 minutes
U937
Normalized mean fluorescent intensity (to untreated)
2.5
2.0
1.5
1.0
0.5
0.0
*
Veh
AMD 3100
BL-8040
CXCL12 -LD
B
24 hours
Normalized mean fluorescent intensity (to untreated)
2.0
1.5
1.0
0.5
0.0
*
Veh
AMD 3100
BL-8040
CXCL12 -LD
C
AML 193
Normalized mean fluorescent intensity (to untreated)
1.5
1.0
0.5
0.0
*
Veh
AMD 3100
BL-8040
CXCL12 -LD
D
Normalized mean fluorescent intensity (to untreated)
2.5
2.0
1.5
1.0
0.5
0.0
*
Veh
AMD 3100
BL-8040
CXCL12 -LD

Figure 7.

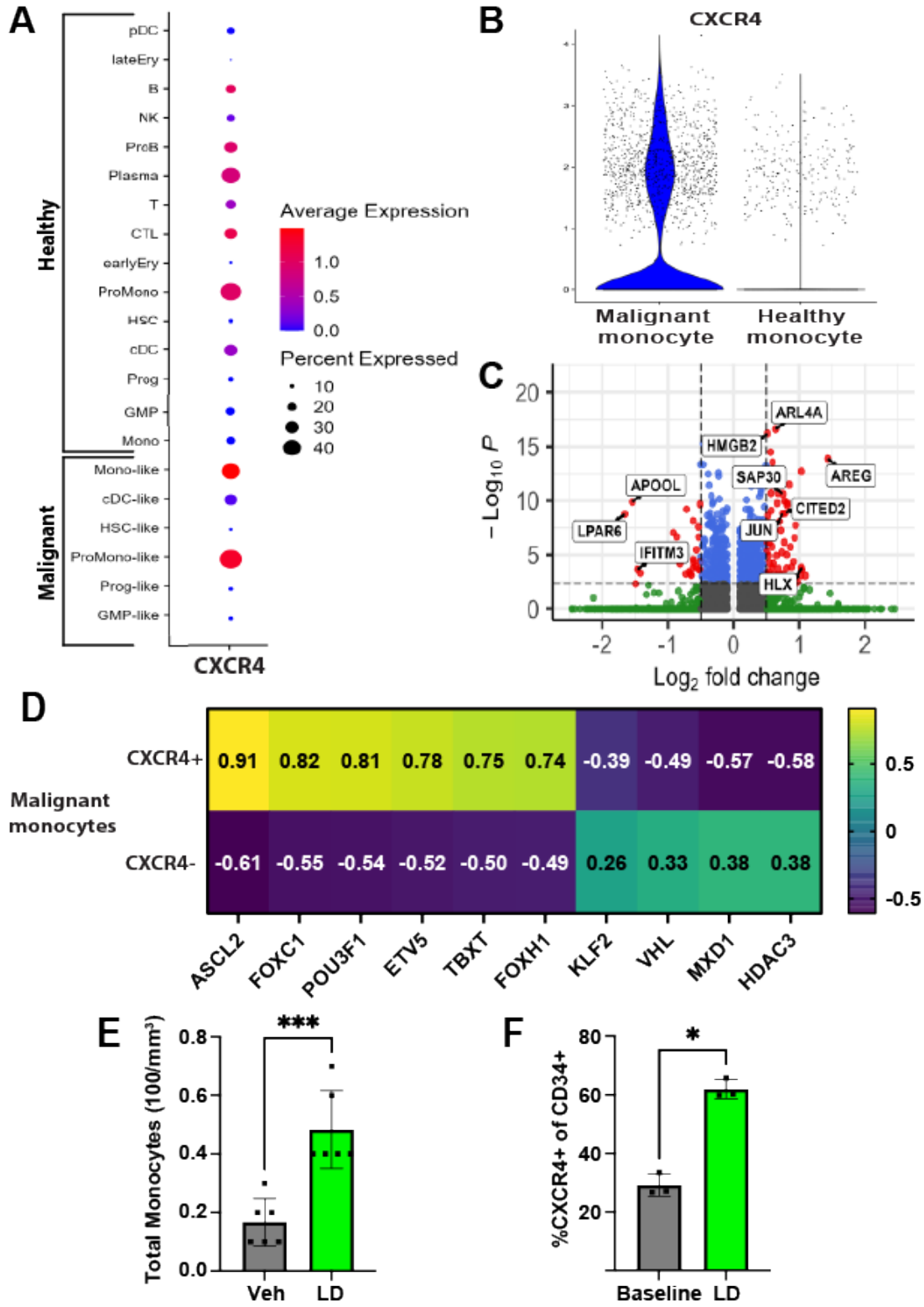
A
Healthy
Malignant
pDC
lateEry
B
NK
PreB
Plasma
T
CTL
earlyEry
ProMono
HSC
cDC
Prog
GMP
Mono
Mono-like
cDC-like
HSC-like
ProMono-like
Prog-like
GMP-like
CXCR4
Average Expression
1.0
0.5
0.0
Percent Expressed
10
20
30
40
B
CXCR4
Malignant monocyte
Healthy monocyte
C
ARL4A
HMGB2
SAP30
AREG
APOOL
CITED2
LPAR6
JUN
IFITM3
HLX
$-\text{Log}_{10}$ P
Log_2 fold change
D
Malignant monocytes
CXCR4+
0.91 0.82 0.81 0.78 0.75 0.74 -0.39 -0.49 -0.57 -0.58
CXCR4-
-0.61 -0.55 -0.54 -0.52 -0.50 -0.49 0.26 0.33 0.38 0.38
ASCL2
FOXC1
POU3F1
ETV5
TBXT
FOXH1
KLF2
VHL
MXD1
HDAC3
E
Total Monocytes (100/mm³)
***
Veh
LD
F
%CXCR4+ of CD34+
*
Baseline
LD

Figure 8.

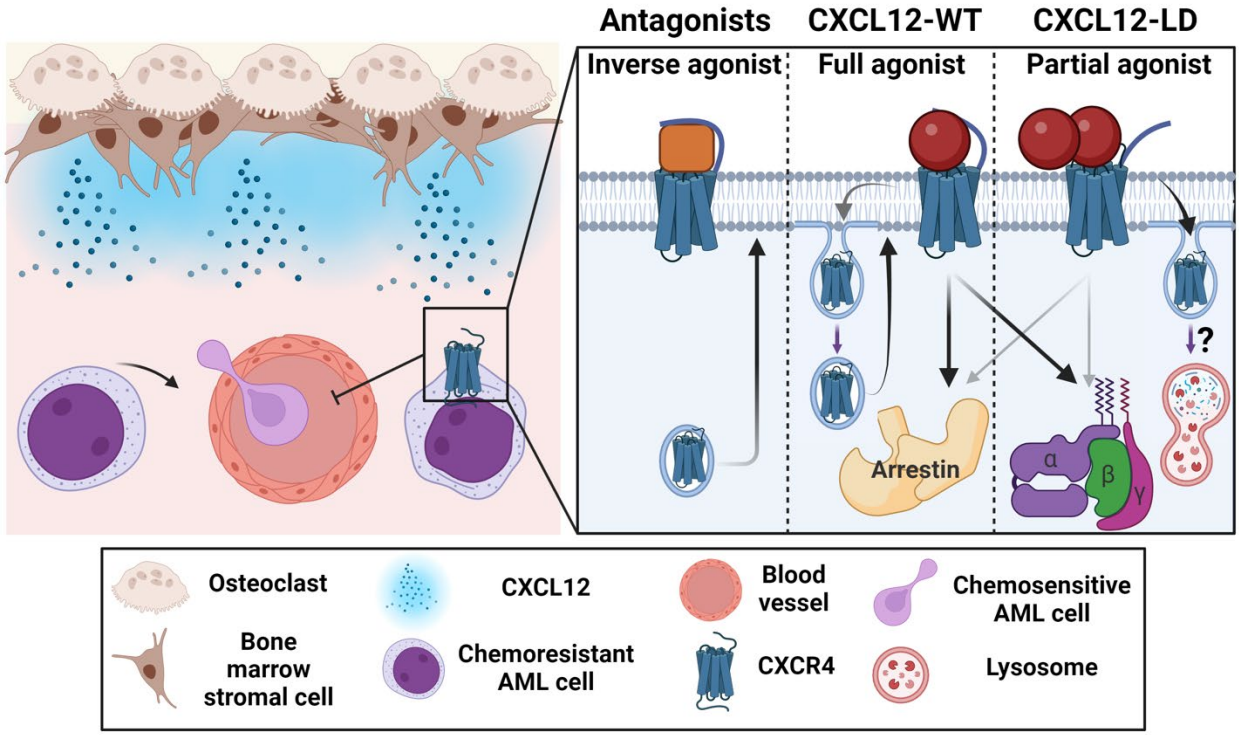
Antagonists
CXCL12-WT
CXCL12-LD
Inverse agonist
Full agonist
Partial agonist
Arrestin
α
β
γ
?
Osteoclast
CXCL12
Blood vessel
Chemosensitive AML cell
Bone marrow stromal cell
Chemoresistant AML cell
CXCR4
Lysosome